

1 **Fracture patterns associated with the evolution of the Teton anticline, Sawtooth Range, Montana,**
2 **USA**

3

4 Authors: C.M. Burberry^{1,2}, D.L. Cannon^{3,4}, J.W. Cosgrove², T. Engelder⁴

5 1 – University of Nebraska-Lincoln. 2 – Imperial College London. 3 – Diamondback Energy. 4 – The
6 Pennsylvania State University

7

8 **Abstract**

9 The Teton anticline and adjacent structures at the deformation front of the Sawtooth Range
10 fold-thrust belt in Montana are fractured in such a way that some have used these as a model for the
11 fractures that propagate during buckle folding. However, advances in understanding both the process
12 of folding in forelands and the evolution of fracture patterns found within these folds suggests that it is
13 time to reinterpret the nexus between fracturing and folding within this classic structure. Data
14 gathering includes two steps starting with the documentation of the along-strike changes in the
15 geometry of the Teton anticlines, using field measurements, aerial photographs and seismic lines, and
16 then the collection of fracture orientation data and abutting relationships. With the benefit of seismic
17 lines, Teton anticline is best described as a fault-related fold, forming in response to changes in the
18 underlying ramp and flat geometries. The propagation of joints (mode I cracks) initiated with formation
19 of two major sets whose orientation is controlled by pre-folding, regional stresses. Two more joint sets
20 propagated in local stress fields, developed in response to the growth of fault-related folds. Some early
21 joints were reactivated as wrench faults during amplification and tightening of the anticlines. The
22 fracture sets identified in this study are consistent with two unrelated mechanisms starting with
23 propagation in a regional stress field. This first mechanism is poorly understood but might be related to
24 regional stretching in the Sawtooth Range orocline. The second mechanism is associated with tangential
25 longitudinal strain during anticline development. Thus, we suggest that fracture networks across folded
26 hydrocarbon reservoirs should be interpreted and characterized in the light of a more complex tectonic
27 setting and the genetic or geologic history of the system as a whole.

28

29

30 1. Introduction

31 Teton anticline, in the Sawtooth Range, Montana, is the source of a popular model for fracture
32 development associated with buckle folds, (Fig. 1; Stearns, 1964; Stearns, 1968; Friedman and Stearns,
33 1971). On the basis of their studies focused primarily on the geometric relationship between the
34 fractures and the fold, Stearns and Friedman (*op. cit.*) recognize five conjugate systems of macro-
35 fractures. These five macro-fracture systems presumably formed because buckle folding forced an
36 exchange of principal stress axes at various localities within the fold during the growth of Teton
37 anticline. During the half century which has elapsed since the original Teton anticline work, and
38 contemporaneous work on the Cardium Sandstone utilizing similar ideas (Muecke and Charlesworth,
39 1966), ideas on deformation linked to evolving fold-thrust belts (Marshak et al., 1992) and models for
40 fold-related fracturing have proliferated.

41 For example, Lorenz et al. (1991) distinguish between regional fractures and fold-related
42 fractures, with the regional fractures forming parallel to far-field regional compression at depth.
43 Jamison (2016) revisits the Cardium Sandstone field area of Muecke and Charlesworth (1966), and
44 generates a fracture model after the Stearns (1968) style, invoking increased complexity in fold style to
45 create increased complexity in fracturing. His model notes reactivation of extensional fractures in shear,
46 as well as formation of initial conjugate shear fractures. A model from Bellahsen et al. (2006) also
47 describes pre-folding regional fractures and fold-related extension and shear fractures for the Sheep
48 Mountain Anticline, WY. Clearly, early joint sets pre-date folding even in Laramide settings (Laubach,
49 1992; Hennings et al., 2000; Silliphant et al., 2002; Bergbauer and Pollard, 2004; Bellahsen et al., 2006;
50 Ahmadhadi et al., 2007) and as detachment folding evolves multiple joint sets develop (Srivastava and
51 Engelder, 1990; Engelder et al., 1997; Sanz et al., 2008). Still the connection between transverse joints
52 (i.e. vertical joints approximately normal to the fold axis) and folding is unresolved. Bergbauer and
53 Pollard (2004) show that the presence of pre-folding fractures can strongly influence the orientation of
54 fold-related fractures, using a case study from Emigrant Gap anticline, WY. Similarly, Ahmadhadi et al.
55 (2007) and Lacombe et al. (2011) show pre-folding, syn-folding and fault-related fracture sets across
56 folds in the Zagros Simply Folded Belt, where the former affects the orientation of the latter. In the
57 Zagros folds, the model of Cosgrove and Ameen (1999) for fracture complexity formed on the forelimbs
58 of fault-related folds is also referenced. Casini et al. (in press) note that an axis-parallel fault system can
59 develop in anticlines in the Zagros Simply Folded Belt due to outer arc extension, as well as the sets
60 noted by Ahmadhadi et al. (2007), Lacombe et al. (2011) and Cosgrove and Ameen (1999).

61 Curvature is often used as a predictor of fracture intensity and the orientations of fracture
62 networks, see e.g. Lisle 1992 & 1994. Fischer and Wilkerson (2000) demonstrate that if sedimentary
63 layers are treated as elastic plates, joints open parallel to the maximum instantaneous stretch (the
64 maximum curvature) of a layer and trend parallel to the minimum instantaneous stretch (minimum
65 curvature) of that layer. Thus, joints across folds are a reflection of the evolution of the curvature of the
66 structure during its evolution, rather than simply the product of the final curvature of the surface.
67 Watkins et al (2015) demonstrate that in high curvature regions, fractures are high intensity, short and
68 oriented parallel to fold hinge lines. In low curvature regions, fractures are more continuous and show a
69 variation in orientation, maybe influenced by lithological variations (Watkins et al., in press). They
70 suggest that in high strain regions fractures are more consistent and predictable, typically oriented
71 parallel to strike or to local faults, than in low strain regions. Still, there is no consensus on fracture
72 genesis in folded regions.

73 With regard to the Teton Anticline, seismic sections have confirmed that the anticline is a fault-
74 bend fold linked to thrust ramps (Suppe, 1983; Holl and Anastasio, 1992) rather than a buckle fold. In
75 addition, criteria for identifying fractures and systems of macro-fractures have evolved to the point that
76 they no longer support the old conjugate fracture system model (Pollard and Aydin, 1988).
77 Furthermore, these criteria enable a determination of the chronology of the various fracture sets
78 making up cumulative fracture networks which were once considered contemporaneous conjugate
79 fractures (Younes and Engelder, 1999). The new insights into the origin of the Teton anticline and the
80 availability of criteria for sorting out the evolution of fracture sets found within the anticline, motivated
81 the present authors to re-examine this classical structure.

82 The critical objectives of our paper are (i) to document the surface and subsurface geometry of
83 the anticline pair (the Teton and Little Teton anticlines) situated near the leading edge of the Sawtooth
84 Range, Montana, and (ii) in the light of the reinterpretation of the origin of the Teton anticline as a fault-
85 related fold, to re-evaluate the nature and origin of the systems of conjugate macro-fractures identified
86 in previous studies. Since the original study is still used as the basis for many fracture interpretation,
87 modelling or prediction studies (e.g. Cooper et al., 2006), we anticipate that our reinterpretation and
88 conclusions will have wide-ranging relevance to the hydrocarbon industry. Another objective of this
89 paper is to investigate the role of lithology in controlling joint development in a foreland, particularly
90 when the fractured rocks are not sandwiched between organic rich rocks. The Teton anticline fold
91 model is based on observations in the relatively massive carbonates of the Madison Formation, Fig. 2, 3.

92 Yet, the anticline and an adjacent fold, the Little Teton anticline, carry a blanket of clastic rocks over the
93 Madison Formation. The clastic section did not detach from the Madison Formation and thus has much
94 the same fold history as the carbonates. An understanding of joint development in the clastic cover may
95 give further insight into the sequence and timing of fracture development in the carbonates of the
96 Teton anticline.

97

98 **2. Geologic Background**

99 The Teton anticline falls within the Northern Disturbed Belt of Montana, formed during the
100 Sevier Orogeny between 140 and 85 Ma (Cooper 1992, DeCelles 2004) (Fig. 2). The Northern Disturbed
101 Belt has four distinct provinces, from west to east, the Flathead Range Complex, Sawtooth Range
102 Complex, Sun River Valley Complex and High Plains Province (naming convention of the present authors)
103 corresponding to the four sub-belts of earlier work (Mudge, 1982a). The largest hinterland thrust sheet
104 in the region, the Lewis-Eldorado-Hoadley sheet, forms part of the Flathead Range Complex. This thrust
105 sheet has had several phases of movement, including one phase synchronous with thrusting in the
106 Sawtooth Range, an event which generated the two anticlines of the study area (Crider, 1993; Crider
107 and Boyer, 1993). The Sawtooth Range Complex is a thin-skinned, foreland fold and thrust belt,
108 consisting, in the region studied, of north-south striking, closely spaced, westerly dipping imbricate
109 thrust sheets that have been subsequently folded (Mudge, 1970, Boyer and Elliott, 1982). The
110 dominant detachment surface in the Sawtooth Range appears to step up-section, from the Middle
111 Cambrian Gordon and Switchback Formations in the hinterland, to the Devonian Jefferson-Three Forks
112 Formations close to the western boundary of the Sawtooth Range Complex (Fig. 3). Subsequently, this
113 detachment steps further up section to the base of the Lower Cretaceous section within the frontal
114 deformation zone (Singdahlsen 1984, Holl and Anastasio, 1992).

115 The southern portion of the Northern Disturbed Belt is underlain by the northeast-trending
116 Great Falls Tectonic Zone (GFTZ) which is a 250 km wide zone of intense basement deformation
117 stretching from the Idaho batholith into Saskatchewan (Boerner et al., 1998; Finn and Sims, 2005) (Fig.
118 1). Deformation within the GFTZ involves a series of high angle faults and shear zones, with dyke
119 swarms, gravity and magnetic anomalies and thickness changes in the Phanerozoic sediments (O'Neill
120 and Lopez, 1985). The Great Falls Tectonic Zone is interpreted as an Archean shear zone separating the
121 Wyoming block to the SE and the Medicine Hat block to the NW. It has been periodically reactivated

122 since the Proterozoic and possible as late as the Holocene (O'Neill and Lopez, 1985, Boerner et al.,
123 1998). Specific lineaments within this tectonic zone referenced in this paper and shown in Fig. 1, are the
124 Scapegoat-Bannatyne Trend, the Pendroy Fault zone and the Brown Sandstone Peak-Brady trend and
125 these appear to have influenced the strike of the Sawtooth Range Complex thrusts, e.g. close to Augusta
126 (Mudge, 1982a, Reinecke, 1989, Holl and Anastasio, 1992).

127 **2.1 The Teton Anticlines**

128 The Teton Canyon area is located 30 miles NW of Choteau, Montana (Fig. 2). At this point, the
129 Teton River which flows from west to east, has two major tributaries (i.e., the Teton North Fork and the
130 Teton South Fork) which have carved canyons into the local structures (Fig. 4). These E-W trending
131 canyons provide cross sectional exposures through the N-S trending Teton and Little Teton anticlines,
132 which mark the deformation front of the Sawtooth Range in this area. These two anticlines have been
133 interpreted as frontal ramp anticlines by Mudge (1982b) and as buckle folds with broad hinges,
134 separated by an unfaulted syncline, by Stearns (1964 & 1968). The larger of the anticlines, the Teton
135 anticline, plunges and dies out to the south. In contrast, approximately 10 km north of the canyon,
136 where the foreland thrust system in the Cretaceous section becomes more complex, (Mudge and
137 Earhart, 1983) this anticline terminates against the Volcano Reef thrust (Fig. 4).

138 The units involved in deformation within the Teton Canyon study area are the Upper Devonian
139 and younger units (Figs. 2 & 3). Collectively, the Devonian and Mississippian units represent a shallowing
140 upwards shoreline sequence, culminating in a shallow lagoon-like environment on a Mississippian
141 rimmed shelf on the western craton margin, between the Antler Orogen to the west and the Trans-
142 continental Arch to the east (Sando, 1976). The Mid-Late Jurassic Ellis Group lies disconformably on
143 the Mississippian Madison Formation, with a time gap of 140 my. The Ellis Group contains evidence of a
144 marine transgression, backarc uplift and sabkha or tidal flat environments as well as shoreline fluvial
145 systems (Dickinson and Gehrels, 2003). This Group is unconformably overlain by the Upper Jurassic
146 Morrison formation, which is considered to be the backbulge sediments of a classic, foreland basin
147 system, as thrusting began to the west (DeCelles, 2004). The basal Cretaceous unconformity represents
148 the migration of the forebulge towards the east, modified by dynamic subsidence of the lithosphere.
149 The Mount Pablo and Kootenai formations were deposited in the foredeep. These sequences are
150 entirely non-marine. In the Aptian, marine inundation began as the Cretaceous Interior Seaway
151 engulfed the foreland basin system, depositing the Colorado Group Shale. Thickness variations within

152 the Colorado Group Shale imply a palaeo-high in the Teton Canyon region, probably related to the Great
153 Falls Tectonic Zone (Lorenz 1982).

154 **2.2 Fractures at the Teton Anticlines**

155 At Teton anticline the original model for fold-related fracturing identified five conjugate fracture
156 sets which would have formed as the fold evolved through several stress states. Later mapping of
157 fractures at Teton Anticline confirmed that, with the exception of transverse shear zones developed
158 with a spacing of 10s to 100s of meters, all steeply dipping (relative to bedding) fractures are joints
159 (extension fractures) (Ghosh and Mitra, 2009). There are, however, abundant low angle faults (relative
160 to bedding) in the region that may have developed as shear fractures from the onset rather than
161 evolving as joints reactivated in shear (Holl and Anastasio, 1992). The more recent analysis of bedding-
162 normal and bedding-subnormal fractures at Teton Anticline document four sets of 'extension' fractures
163 (Ghosh and Mitra, 2009). The two more common sets are roughly longitudinal and transverse to the
164 fold with the less common sets being oblique to fold axes. Ghosh and Mitra (2009) interpret their data in
165 terms of curvature: "the variation in curvature of the folded surface can be used to explain the
166 distribution of densities of longitudinal fractures". Stretching to failure is a common assumption in
167 many models that assume a correlation between curvature and fracture density (Fischer and Wilkerson,
168 2000; Hennings et al., 2000). Ghosh and Mitra (2009) explain the propagation of transverse joints using
169 the same driving mechanism, "probably related to curvature parallel to fold axis caused by variations in
170 fold plunge".

171

172 **3. Methods, data and analysis**

173 Our study of fracture development associated with the along-strike variation of the Teton
174 anticline was carried out using a combination of geophysical data and field measurements. The
175 geophysical data set consists of a series of E-W trending seismic lines crossing the study area, obtained
176 courtesy of Seismic Exchange Inc. The data is stacked, but not migrated and therefore contains pull-up
177 artifacts and unusually steep dip sections on faults. Formation top data from exploration wells in the
178 area, made available by the Montana Board of Oil and Gas, allowed key units to be picked at depth and
179 correlated to surface exposures on one key seismic line. The seismic interpretations were combined
180 with the field data concerning the surface anticline geometry, in order to create a series of cross-
181 sections and geometric and genetic models of the anticline structures.

182 The surface geometry of both the Teton and Little Teton anticlines was mapped for
183 approximately 6 km along their strike, from a thrust cut-off at the Volcano Reef thrust in the north, to a
184 point just south of Teton Canyon (Fig. 3). The area covered was approximately 20 km². Data were
185 collected at 225 stations within this area and at each station, the location was recorded using a GPS
186 receiver. The orientation and lithology of the anticline surface were recorded. Where possible,
187 orientation data on brittle structures were collected, along with observations of abutting relationships
188 between fractures and any kinematic indicators such as mineral lineations.

189 Mesoscopic-scale brittle structures were sorted into mini-joints, common joints (i.e. large-scale
190 joints), large-scale fractures exhibiting slip, and brittle shear zones, mainly wrench fault zones, several
191 meters wide. Mini-joints were distinguished from common joints by a series of criteria, including
192 proximity to stylolites, non-systematic orientations, and strike length where common joints are
193 unrelated to stylolites, are found in systematic sets and have a strike length > 0.5 m. In total,
194 orientation data were collected on 1757 common joints, distributed among 160 stations. The
195 orientation data were collected on pavement surfaces where it was possible to measure both strike and
196 dip with confidence on less than 50% of the fractures. Otherwise, we gathered just the strike of the
197 fracture. In order to enable better visualization of joint sets when clustering of sets was weak, full
198 orientation data were plotted as both poles and planes in lower hemisphere stereographic projection.
199 Both the complete orientation data and strike data were combined in rose diagrams of common joints.

200 Mini-joints were only found in the pelagic mudstones of the upper member of the Castle Reef
201 Dolomite. These are not exposed as surfaces and consequently only orientations of approximate strike
202 direction, (the intersection lineation they make with the exposure surface), could be collected. At 5
203 stations in the lower parts of the Morrison Formation, particular attention was paid to the common
204 joints in and around a series of carbonate concretions. Additional data recorded at these stations noted
205 whether the measured common joint was contained within the concretion, was found only in the matrix
206 material, or was found in both concretion and matrix.

207 The data on brittle structures were analyzed and used to identify prominent fracture
208 orientations, and to categorize the fractures into the various classes of brittle structures described
209 earlier. In order to analyze the 'common joint' dataset, the Teton anticline (TA) was divided into
210 traverses. The northern traverse is that part of the study area north of the North Fork of the Teton
211 River. The central traverse is the area between the two forks of the Teton River, and the southern
212 traverse is the area south of the South Fork (Fig.4). The northern traverse of the anticlines contains the

213 cross sections shown in Fig. 5A and X-X' in Fig. 4, the central traverse contains the cross sections shown
214 in Figs. 5B and 5C and the southern traverse contains the cross-section shown in Fig. 5D. Within each of
215 these traverses, datasets from the forelimb, backlimb and, where possible, the hinge region, were
216 gathered and analyzed separately. Similarly, the Little Teton anticline (LTA, Fig. 4) is divided into two
217 traverses, the plunging nose (located east of the central traverse of the TA) and the more symmetrical
218 and cylindrical northern traverse. The northern traverse dataset was separated into forelimb and
219 backlimb categories for analysis.

220 Additionally, the age relationship of fracture sets were determined on the basis of their abutting
221 relationships and the dataset from the Morrison Formation concretion stations. Lastly, these results
222 were combined with the geometric and genetic anticline models, to produce a geologic history for the
223 anticlines that incorporates the stages of fold growth, and the generation and interaction of fracture
224 sets at each stage.

225

226 **4. Subsurface geometry of the Teton Anticlines**

227 Analysis of the orientation data from the anticline surfaces in the study area indicates that the
228 average strike of the Teton anticline (hereafter TA) is slightly west of north, although there is a subtle
229 change in strike near the South Fork of the Teton Canyon. The smaller of the two anticlines, Little Teton
230 anticline (hereafter LTA) has an average strike of 173°. Dip data was divided into dip domains and the
231 anticline geometries were constructed from these dip domains using a kink-method approach (Suppe,
232 1985). The unit used as a marker layer in Fig. 5 is the "J_{sr}", the lowest two Formations of the Jurassic
233 clastic succession (Fig. 3). This unit was chosen because the contact between this unit and the
234 underlying Mississippian Madison Formation forms the presently exposed surface of the anticlines and is
235 thus mappable across most of the field area.

236 **4.1 Cross-sections from field data**

237 The four cross-sections shown in Fig. 5 give an indication of the extent to which there is a
238 change in anticline geometry along strike. In the northern part of the study area the TA has a broad,
239 sub-horizontal hinge region, with limbs dipping at approximately 20° W and 18° E (Fig. 5 A). The axial
240 surface is inclined, dipping steeply to the west. The LTA has a more rounded hinge region, with limbs
241 dipping at approximately 18° W and 15° E. The axial surface of this anticline also dips steeply west. 2
242 km further south the TA has a more rounded hinge region, with limbs dipping at approximately 25° W

243 and 24° E (Fig. 5B). The axial surface is inclined, dipping steeply to the west. The LTA also has a rounded
244 hinge region, with limbs dipping at approximately 25° W and 35° E. The axial surface of this anticline
245 also dips steeply west. Within the north fork of the Teton Canyon 2km further south of cross-section B,
246 the TA has a rounded hinge region and a smaller inter-limb angle than further north (Fig.5 C). The axial
247 surface is still steeply inclined to the west and the anticline limbs dip at approximately 27° W and 54° E.
248 The LTA still has a rounded hinge region on this section, although the anticline has a lower amplitude,
249 since this cross-section is located close to the nose of the anticline. The limbs dip at approximately 17°
250 W and 16° E. Cross section D is drawn close to the south fork of the Teton Canyon 2km further south
251 than cross-section C (Fig. 5 D). The asymmetry of the TA is more pronounced and the hinge region is
252 broader than in cross-section C but not as broad as in the northernmost cross-section (Fig. 5 A). The
253 anticline limbs dip approximately 24° W and 60° E and the LTA dies out before reaching this section.
254 South of this cross-section, a saddle develops in the crest of the Teton anticline and the anticline hinge
255 line, which is approximately horizontal in the four sections shown in Fig. 5, plunges 15° to the south into
256 the saddle region. Once the saddle has been crossed the anticline plunges gently to the north.

257 **4.2 Seismic cross-sections across the Teton anticlines**

258 Seismic data across the region indicate that, despite limited surface evidence of emergent
259 thrusts related to these anticlines, the deep structure consists of a series of stacked thrust sheets (Fig.
260 6). This seismic line is located close to the cross-section in Fig.5 B and line X-X', Fig. 4. Combined with
261 well data (the location of which is shown on Fig. 4) two additional thrust sheets, carrying both the
262 Mississippian and Jurassic-Lower Cretaceous sections, can be identified beneath the thrust sheet
263 carrying the TA and LTA (here named the Crab Butte thrust or CBT). The detachment for these thrust
264 sheets is identified on the basis of well data, to be in the Upper Devonian units, probably the Three
265 Forks Formation, as indicated on Fig. 3.

266 Expanding the interpretation to include all the available seismic lines indicates that the
267 subsurface thrust sheets also change in configuration from north to south within the field area. Two
268 representative interpreted lines are shown in Fig. 7 (a & b). The line labeled Line 1 in this figure is the
269 same line as that shown in Fig. 6. The seismic section on which Fig. 7b is based was shot south of the
270 study area (see e.g. Fig. 4) and thus south of section D, Fig. 5. This line shows that the CBT is emergent in
271 the foreland i.e. to the east of the TA, and that a smaller thrust splay (here named the Pine Butte thrust
272 or PBT) cuts the forelimb of the TA which is highly asymmetric at this locality. Additionally, whereas the
273 CBT detachment is found in the Devonian section in Line 1, it can be seen from Line 2 that, in this

274 section, the CBT originates from a deeper detachment surface found towards the base of the Cambrian
275 section, potentially within the Gordon Formation (Fig. 3). This deeper detachment surface explains the
276 presence of the Cambrian section in an exploration well at the crest of TA, close to this line (Fig. 7b).

277 **4.3 Interpretation**

278 The above data indicate that the TA changes significantly in geometry along strike, most
279 particularly with respect to the geometry of the E-dipping forelimb. This limb becomes more steeply
280 dipping as the anticline is traced southwards, becoming considerably steeper south of the north fork of
281 the Teton Canyon. The backlimb has a more constant dip than the forelimb, but it too displays a steeper
282 section close to the south fork of the Teton Canyon. The LTA shows a near-symmetrical geometry,
283 consistent with a smaller anticline structure that dies out close to the northern and southern margins of
284 the mapped area by plunging gently to the north and south respectively. It should be noted that the
285 southern dying-out of this structure corresponds with the marked steepening of both limbs of the
286 adjacent, larger, TA. Additionally, it is clear from the geometry of the structures revealed by the cross
287 sections shown in Figs. 4 & 5 and the seismic sections on which they are based, e.g. Fig. 6, 7a & 7b, that
288 the TA and LTA are either fault-bend folds, or fault-propagation folds (Fig. 7 c & 7 d respectively) i.e.
289 fault related folds rather than classical buckle folds.

290 With these features in mind, we propose that the TA is in fact made up from two folds linked
291 together along strike. The linkage zone is proposed to be around the South Fork of the Teton River, a
292 fact that will become important in our proposed fracture model. By combining the measurements and
293 analysis of the surface data, and a depth model based on the seismic interpretations, we identify a
294 crucial location: the position along the Teton anticline where a marked asymmetry in the profile occurs
295 and the point where the LTA plunges towards the south to die out. Both locations occur in the region of
296 the study area where thrust sheet geometry varies considerably (c.f. Fig. 7 a & b). Moving south from
297 Line 1 to 2, the lower detachment in the imbricate thrust sheets becomes deeper in the sedimentary
298 succession. This region, essentially the south fork of the Teton Canyon, appears close to the Brown
299 Sandstone Peak-Brady trend in the basement (Fig. 2). Given these observations, we propose a three-
300 stage model for the development of the TA and LTA anticlines. During initial fold amplification, the TA is
301 considered to be two separate anticline structures, one in the north of the study area (north of the
302 North Fork of the Teton River) and one in the south (south of the South Fork of the Teton River). LTA is
303 also present to the east of TA, in the northern part of the study area. The Teton River flows between the
304 two anticlines that will eventually link to form the present-day TA. As anticline amplification continues,

305 both proto-TA anticlines propagate along strike towards each other and become linked, forming a
306 saddle in the structure in the south fork of the Teton Canyon. This saddle is located above the major
307 lateral ramp in the CBT, and the Brown Sandstone Peak-Brady trend. During the final stage of fold
308 development, shortening continues to be accommodated across the now-combined TA structure, and
309 wrench faults form in the saddle region (see section 5). The LTA does not continue to propagate
310 southwards, and as a result the shortening across the area south of the saddle region is taken up by
311 tightening and the development of marked asymmetry in the main TA structure.

312 **5. Fractures and related features around the Teton anticlines**

313 To understand the nature of joint development in the Sawtooth foreland and its connection
314 with fold growth, fracture data were grouped according to structural position (forelimb and backlimb)
315 and traverse across each anticline (i.e., the north, central, and south traverses), as well as divided by
316 lithology (clastic or carbonate). We tried three forms of data presentation for common joints by
317 separating the fracture data based on whether the host was a clastic or carbonate rock or making a
318 composite by combining the clastic and carbonate data. The former was plotted as both contour
319 diagrams of poles to joints and lower hemisphere projections of the joint planes. The composite data
320 were plotted as rose diagrams combining complete orientation data and those data for which just the
321 strike of the fracture is known. When appearing alone, none of the three data displays gives as
322 complete a picture as plots showing all three representations together. Thus our findings are based the
323 combination of three presentations.

324 **5.1 Teton anticline northern traverse**

325 The northern traverse across TA provides a picture of the basic joint sets against which other
326 traverses may be compared (Fig. 8). A rose diagram of backlimb data combining fractures from both
327 carbonates and clastics suggests that TA contains two prominent fracture sets (Fig. 78a). One set,
328 henceforth known as the longitudinal set, is oriented with a mean strike of 166° . The other set is
329 henceforth known as the transverse set, and has a mean strike of 077° . The transverse joints are more
330 widely dispersed about the mean value on the rose diagram and appear to have three discrete peaks
331 within the overall transverse orientation.

332 When plotted as planes in lower hemisphere projection some subtle trends emerge for the
333 backlimb data, particularly when joints are sorted by host lithology, carbonate or clastic (Fig. 7b). First,
334 the mean strike of longitudinal joints in carbonates differs by more than 5° anticlockwise from the fold

335 axis (dashed lines on Figs. 8b & c etc.) and this set has a dip of 85° to the west. The mean strike of the
336 longitudinal joints in the clastic units deviates by about 5° clockwise from the fold axis. The dispersion
337 within the transverse joint set, in both clastic and carbonate units, is high. In the carbonate units, it is
338 possible to discern a more E-W set ($\approx 85^{\circ}$) tending to dip to the north and an ENE set ($\approx 75^{\circ}$) tending to
339 dip to the south. In the clastic units, a NW-dipping NE-oriented set may be discerned ($\approx 65^{\circ}$) and the
340 distribution of joints in the carbonate units allows the possibility that this set may also be present, albeit
341 less well-developed. We contend, then, that there are three sets of transverse joints developed,
342 together with a longitudinal joint set, at this traverse of TA.

343 Despite a smaller number of data in the forelimb, we see the same trend for longitudinal joints
344 as recorded in the backlimb (Fig 8 a, c). However, the mean strike of the longitudinal joints and the fold
345 axis are about the same. The transverse joints are dispersed leaving the possibility of more than one set
346 like the backlimb. This possibility is most evident when considering the clusters of poles for the
347 carbonates of the forelimb – three separate clusters can be identified in Fig. 8 c.

348 In carbonates of the hinge region of the northern traverse, longitudinal joints abut the $\approx 85^{\circ}$
349 joints (Fig. 9a), indicating that the transverse joints are older. At a different station along the northern
350 traverse, the longitudinal joint set abuts the $\approx 65^{\circ}$ joints (Fig. 9b). These transverse orientations fall
351 within the range of the two transverse joint sets seen in orientation plots shown in Fig. 8. In the
352 carbonate units of the hinge region, abutting relationships between these two sets of transverse joints
353 were not observed.

354 **5.2 Teton anticline central traverse**

355 The joint pattern on the backlimb of the TA in the central traverse is similar to that in the
356 northern traverse with transverse and longitudinal joints in the orientations as described above (Fig.
357 10a). Longitudinal joints are also well-developed in the forelimb, and transverse joints have the same
358 dispersion with orientations ranging from $\approx 60^{\circ}$ to $\approx 90^{\circ}$. The joint pattern from the clastic section in the
359 backlimb shows two transverse sets but with a wider dispersion (Fig. 10b). The dispersion of transverse
360 joints in clastic rocks of the forelimb is about the same but with the most prominent set having an E-W
361 strike (Fig. 10c).

362 In both the central and northern traverses, a set of large-scale sub-vertical faults can be
363 observed, which appear as conjugate pairs marked by tree lines on the limbs and hinge zone of TA (Fig.
364 11). These tree lines are sometimes identifiable in the field, and orientations of these tree lines were

365 measured where possible. No dip data was collectable at these sites. There are tree lines sub-parallel to
366 the longitudinal joint set (oriented at 155°) and a set of transverse tree lines oriented at $\approx 70^\circ$. There
367 are additional other prominent directions on these tree lines, oriented at $\approx 60^\circ$, $\approx 90^\circ$ and $\approx 180^\circ$. The
368 slight variation in mean longitudinal and transverse orientations between these tree lines and the other
369 joint data is inferred to be a result of the different scales of measurement, an issue noted by McQuillan
370 (1973) and probably not significant for the purposes of this study.

371 **5.3 Teton anticline southern traverse**

372 In the southern traverse of TA there were fewer outcrops so the plots in Fig. 10 e & f show less
373 pronounced clustering than plots from the northern traverse. The joint data from the Castle Reef and
374 Allan Mountain Formations come mainly from the hinge of the anticline. The longitudinal joints in the
375 southern traverse of Teton Anticline are in the same orientation as in the northern and central traverses
376 (Fig. 10d-f). The transverse joints are dispersed with a concentration at $\approx 110^\circ$. A hint of this joint set is
377 found in the forelimb carbonates of both the northern and central traverse. In the Mesozoic clastic
378 section of the forelimb joints are dispersed mainly counterclockwise from a prominent set at $\approx 90^\circ$
379 shown by the pole plots in Fig. 10f.

380 On the forelimb of the southern traverse of the Teton Anticline, within the clastic section, sub-
381 horizontal mineral lineations can be found on fractures of the transverse joint set (Fig. 12a). These
382 mineral lineations indicate a wrench-fault sense of movement. Fractures oriented in the transverse
383 orientation, and which show evidence of initial development as opening-mode fractures (i.e., Fig. 12b)
384 followed by subsequent activation as faults with a strike-slip component generating sub-horizontal
385 mineral lineations, are distributed infrequently throughout anticline structures.

386 **5.4 Fractures on Little Teton anticline**

387 LTA plunges to the south with outcrops of the plunging nose of the anticline accessible along the
388 central traverse of the Teton anticlines. Along the northern traverse, LTA is plunging no more than a
389 couple of degrees to the south so the section can be treated like each of the traverses of Teton
390 Anticline. In carbonates of the northern traverse longitudinal joints are sub-parallel to the fold-axis
391 (Dashed line in Fig. 13b) whereas the transverse joints are clustered at $\approx 90^\circ$, although there is
392 dispersion within this grouping that makes this fracture pattern more or less consistent with the
393 northern traverse of TA (Fig. 13a). Two sets of transverse joints may be present with one joint set
394 perpendicular to the fold axis and the other oblique to the fold as much as 10° from the normal to the

395 fold axis (Fig. 12b). Within the clastic section on the northern traverse, the longitudinal joints are again
396 sub-parallel to the fold axis but less tightly clustered than the longitudinal joints in the carbonate
397 section. The transverse joint sets in the clastic section are rotated clockwise relative to the transverse
398 joint sets in the carbonate units.

399 On the nose of LTA, which plunges to the SSW, the joint distribution is dispersed (Fig. 13 c, d).
400 The longitudinal joint set found throughout the Teton Anticlines extends to the nose of LTA where it is
401 not parallel to the azimuth of the hinge line in this part of the fold. Here transverse joints fall within two
402 clusters with strongest clustering oriented $\approx 65^\circ$. This cluster of joints correlates with those joints found
403 in the carbonate units in the northern part of the LTA. No carbonate units were exposed on the nose of
404 LTA.

405 **5.5. Fractured concretions**

406 The Upper Jurassic Morrison Formation (Fig. 3) in the study area contains layers of
407 discontinuous concretionary carbonates between other beds of fine-grained sandstone. Discontinuous
408 concretions in the Morrison Formation have a range of depositional styles. Some concretion-bearing
409 strata develop as broader mats of irregular thickness. In other places concretion-bearing strata are
410 populated with isolated, spherical to oblate carbonate concretions. The encapsulating strata, i.e. the
411 matrix in which the concretions are situated, is composed of fine to medium-grained, greenish-gray
412 sandstone. Weathered concretions show a deep red color.

413 Within the Morrison Formation near the nose of LTA, three separate joint sets cut the
414 concretions; internal joints, external joints, and cross joints. An internal joint set propagates within
415 concretions but does not cut from the concretion into the sandstone matrix. The internal joints within
416 the isolated concretions strike $\approx 85^\circ$. One or two internal joints will populate a concretion and most will
417 traverse the entire concretion (Fig. 14). The internal joint planes are not mineralized but lack
418 recognizable plumose morphology.

419 External joints in the nose of LTA penetrate into the concretion from the sandstone matrix.
420 These joints are several meters long and strike $\approx 65^\circ$. A small percentage of the joints are mineralized
421 with plumose morphology upon the joint plane. External joints are bed normal and thus are rarely
422 vertical. These joints tend to cluster with spacing as close as 8 cm which means that joint spacing is
423 small compared to length. Not all concretions have penetrating external joints while others contain only

424 penetrating external joints. A significant characteristic of external joints is their abrupt termination
425 against internal joints at an acute angle without curving either parallel or perpendicular.

426 The cross joints strike $\approx 181^\circ$ and abut both internal and external joints (Fig. 14). The matrix
427 sandstone contains cross joints similar in orientation as those within concretions. Cross joint planes have
428 nearly vertical dips and small lengths compared to external joints. Most cross joints form between two
429 external joints and terminate at the external joint plane.

430 **5.6 Disjunctive cleavage**

431 The only lithologies that exhibit a well-developed layer-parallel shortening fabric are the
432 carbonates of the Madison Formation. The Allan Mountain (limestone) member carries a disjunctive
433 cleavage that once would have been classified as fracture cleavage (Alvarez et al., 1978). The individual
434 planes are irregular and resemble a longitudinal joint set in outcrop (Fig. 15a). This cleavage dips in the
435 opposite direction (east) as the axial plane of the forelimb of an over-steepened fault-related fold (west)
436 (Fig. 16). Two outcrops carry a cleavage indicative of an E-W shortening whereas the third outcrop
437 exhibits a layer-parallel shortening about 10° south of east. This is in a section of the Teton anticline
438 with an axial plane striking 171° , so there is a mismatch of nearly 20° from anything presumed to be
439 axial planar cleavage (e.g. contrast Fig. 16 outcrop TA 009 data with hinge line orientations in Fig. 10 e &
440 f).

441 In addition to disjunctive cleavage, the Madison Formation is cut by a combination of mini-joints
442 and stylolites (Fig. 17). The stylolites strike sub-parallel to the fold hinge. We have limited dip data on
443 the stylolites, but what there is suggests these may be longitudinal joints that are later stylolitized –they
444 were only found on the hinge region and they are almost bedding normal.

445 **5.7 Interpretation**

446 Across the pair of folds, the most prominent joints constitute three transverse sets $\approx 65^\circ$, $\approx 75^\circ$
447 and $\approx 85^\circ$, and a longitudinal set $\approx 170^\circ$. These four sets are discernable in most carbonate locations on
448 the folds, but the peaks within the overall transverse orientation are sometimes obscured. Within the
449 carbonate units, the longitudinal joints are not always rectilinear with the fold axis, neither are they
450 consistently normal to the most prominent transverse joint orientation. Within the clastic sequence,
451 the longitudinal and transverse joint sets do not mimic exactly in orientation those same sets found in
452 the carbonates, neither are these joint sets rectilinear with the fold axis. The most pervasive joint in the

453 clastic rocks of the forelimb strikes about 10° counter clockwise from its counterpart in the carbonate
454 rocks of the backlimb.

455 In both the clastic and carbonate sections, the longitudinal joints are within a few degrees of the
456 fold axis, so it is possible to make the case that stretching as a consequence of fold curvature was the
457 mechanism for the longitudinal joints. The transverse set is probably made up of three joint
458 orientations, combining to appear as one distributed joint set. This inference is supported by the “fold
459 test” (Fig 18). On unfolding the data from the northern traverse of the TA, the loosely clustered
460 transverse set remains loosely clustered, and on the forelimb, appears to have several sub-peaks within
461 the main cluster (Fig 18, arrowed). The longitudinal data, meanwhile, becomes more distributed on
462 unfolding. This implies that the longitudinal joints are syn-folding, and that the transverse set is made
463 up of some pre-folding and some syn-folding joints. Based on data from the concretions, the $\approx 85^\circ$ set
464 is the earliest of these three sets. Given that longitudinal joint sets also about the $\approx 65^\circ$ set, we infer that
465 this is also a set that is earlier than the main folding event, but later than the $\approx 85^\circ$ set. Thus, the $\approx 85^\circ$
466 and at $\approx 65^\circ$ sets have a pre-folding origin, and are most probably controlled by far-field stresses related
467 to the Sevier orogeny deformation in the hinterland to the Sawtooth Range, before the deformation
468 front had propagated to the study area. The $\approx 75^\circ$ joint set, the third set making up the overall
469 transverse orientation, is interpreted as the cross-fold joint set developed contemporaneously with the
470 longitudinal joint set, during development of the Teton Anticline. Additional dispersion in the transverse
471 data set can be understood as the rotation of fractures that formed at the nose of the anticline, which
472 were then rotated into the limbs as the anticlines propagated towards the linkage zone. These joints,
473 originating sub-parallel to the anticline hinge line, would be rotated into an orientation close to the
474 transverse orientation. Lastly, given that the ‘wrench faults’ are dominantly located in the asymmetric
475 zone of the TA, we suggest that these structures formed during the final stage of anticline development
476 during which time the linkage and tightening of the two segments of the TA occurred as shortening
477 continued.

478 **6. Model for the evolution of fractures across the Teton anticlines**

479 The sequence of fracture development should be considered in light of the model for
480 development of the Teton and Little Teton Anticlines presented in Section 4.3. Prior to the amplification
481 of the anticlines, far field stresses develop transverse fracture sets in the region that will ultimately
482 become the TA and LTA (Fig. 19a). Both the $\approx 85^\circ$ and $\approx 65^\circ$ sets are formed during this period, and
483 presumably reflect an anticlockwise rotation in the far-field stress direction. During amplification of the

484 anticlines, the longitudinal fracture set and the third transverse fracture orientation develop (Fig. 198b).
485 During propagation of the anticlines, joints forming at the nose are rotated into the limbs, and are
486 present now in orientations close to the transverse sets. As anticline amplification continues, both
487 proto-TA anticlines propagate along strike towards each other and become linked, forming a saddle in
488 the structure in the south fork of the Teton Canyon (Fig. 18c). Longitudinal joints continue to form. This
489 saddle is located above the major lateral ramp in the CBT, and the Brown Sandstone Peak-Brady trend,
490 see Fig. 2. During the final stage of fold development, shortening continues to be accommodated across
491 the now-combined TA structure, and accommodation structures (dominantly wrench faults, reactivating
492 pre-existing transverse joints) form in the saddle region (Fig. 19d). The LTA does not continue to
493 propagate southwards, and as a result the shortening across the area south of the saddle region is taken
494 up by tightening and the development of marked asymmetry in the main TA structure.

495

496 **7. Discussion**

497 The Teton anticline is best known as the locality of the classic study of fracture pattern
498 geometry linked to folding (Stearns 1964; 1968). In this paper the interpretation of the fracture sets as
499 structures linked to folding is reassessed. The original work by Stearns has provided the standard model
500 for the link between buckle folds and fractures that has been used by geologists in the hydrocarbon
501 industry for the last 50 years. However, the Teton anticlines have been reinterpreted in this study as
502 thrust related anticlines rather than classical buckle folds as proposed by Stearns (*op. cit.*) and this
503 prompted a reinvestigation of the fracture-fold relationship.

504 The most important sets of fractures observed in the Teton anticlines in the present study are all
505 bedding normal extensional fractures, similar to the finding of Ghosh and Mitra (2009). Their relative
506 ages have been established largely based on distribution throughout the Sawtooth Range and abutting
507 relationships. The joint pattern in and around concretion beds of the Morrison Formation is particularly
508 critical with regard to the timing of joint propagation, and consistent with abutting relationships seen
509 elsewhere. We have presented a model that includes two pre-folding transverse joint sets, syn-folding
510 longitudinal and transverse joints, and includes a stage of tightening in the asymmetric part of the
511 anticline leading to reactivation of joints as wrench faults. The presence of pre-folding fractures is
512 consistent with results from Engelder and Geiser, 1980; Laubach (1992), Hennings et al. (2000),
513 Silliphant et al.(2002), Bergbauer and Pollard (2004), Bellahsen et al. (2006) and Ahmadhadi et al. (2007)

514 which studies span a wide geographic area. Therefore, a regional stress field leading to the generation
515 of fractures, before folding processes occur, should be treated as the expected condition.

516 Concretions within the Morrison carry a second joint set that abuts without curving either
517 parallel to perpendicular to the initial joint set. This lack of interaction between the first and second
518 joint sets suggests that the second set may have originated in the wall of the first. Why there is no
519 apparent interaction by curving as the second joint leaves the first at an oblique angle is unknown.
520 While fracture development in and around the concretions of the Morrison Formation is subtle, this
521 development provides the one clue about the driving mechanism for most, if not all joints in the study
522 area. Models show that joints growing internally within concretions are a consequence of the far-field
523 uniaxial compressive stress generating tensile effective stresses in the vicinity of high modulus
524 concretions (Bessinger, et al., 2003). At depth of burial when concretions fractured in the Morrison,
525 stretching of a softer matrix surrounding the concretion will allow a uniaxial stress state (McConaughy
526 and Engelder, 1989). Otherwise, natural hydraulic fractures driven from the matrix and toward
527 concretions, fail to penetrate the concretion. Once initiated, there is no mechanical reason that a joint
528 originating within the concretion cannot eventually cut outward and into the surrounding matrix.
529 Stretching is a manifestation of the development of an oroclinal bend in the Sawtooth Range in the
530 vicinity of the Teton Anticlines. This same oroclinal stretching is a plausible mechanism for driving
531 transverse joints in the massive carbonates of the Teton Anticlines as well.

532 We note that the forelimb joint patterns are more complex than those on the backlimb, in all
533 sectors of the folds. The intensification of joint propagation on the forelimb of structures is found in
534 other folds (Engelder et al., 1997; Belayneh and Cosgrove, 2004; Sanz et al., 2008). Fracture complexity
535 in the forelimb also implies that a fault may have cored the folds (Cosgrove & Ameen, 1999; Ahmadhadi
536 et al., 2007; Tamara et al., 2015). This fault is not presently drawn on the cross-section to the north of
537 the fold, but is not precluded by our data.

538 The complexity of synfolding fractures is further increased by different patterns in clastic and
539 carbonate successions. We consider three possible explanations for this. First, the clastic succession
540 might have been weaker than the carbonates at the time that the fractures formed, as we suspect
541 relatively early carbonate diagenesis and less rapid burial and diagenesis in clastics (Corbett et al., 1987;
542 Lorenz et al., 2002). Second, there is the possibility that the interbedded sandstones and mudstones of
543 the Swift Unit (Fig. 2) resulted in the folding of these clastic beds by flexural slip or flow. The beds
544 forming the fold are expected to be pinned at the nearest thrust sheet. Third, there is the possibility

545 that the juxtaposition of flexural slip in the clastic section and tangential longitudinal strain in the
546 carbonate succession, led to a more complex fracture pattern (Belayneh and Cosgrove, 2004; Sanz et al.,
547 2008; Smart et al., 2009).

548 In the original interpretation, the four conjugate fracture sets illustrated by Stearns, together
549 with their associated tensile fractures are related to four different stress fields (Fig. 20a – d). An
550 additional group of fractures in the Stearns models (set 5 on Fig. 20g, see also Fig. 1a) is a set of
551 fractures conjugate to the bedding planes, assuming slip on the bedding planes during folding. The
552 hypothesis for the growth of several different conjugate fracture sets during the development of the
553 Teton anticline assumes that the state of stress during anticline growth is forced by boundary conditions
554 into as many as four unique orientations, any and all of which generated a differential stress sufficient to
555 rupture of intact rock in shear. This hypothesis was tested using a variation of the calcite stress meter
556 technique (Friedman and Stearns, 1971; Spang, 1972). The dynamic analysis of calcite twins pointed to
557 only one unambiguous stress state and that was consistent with a conjugate system involving
558 extensional fractures oriented sub-perpendicular to the strike of the anticline (i.e., Set 1, Fig. 20c & g).

559 Of the stress fields associated with the four conjugate fracture sets illustrated by Stearns, only
560 two (i.e., Fig. 20c & d) are appropriately orientated to generate both the anticline and the fractures that
561 have been superimposed onto them. In contrast, the other stress regimes (i.e., Fig. 20a & b), both of
562 which produce extensional fractures parallel to the axial plane of the anticline, are not appropriately
563 oriented to produce an anticline (Fig. 19g). It is argued that these fracture sets (Fig. 20a & b) have been
564 superimposed on an anticline generated by a different, earlier stress field. The stress fields linked to the
565 folding and fracturing (Fig. 20c & d) are regional stress fields. However, during the amplification of an
566 anticline, local stresses can be generated within the layers which modify the regional stress and which
567 may give rise to fractures. Examples of such local stress fields occur in a tangential longitudinal strain
568 fold (Fig. 20e). Such folds characterize the folding of homogeneous, isotropic layers such as the massive
569 limestone beds within the Teton anticline (Ramsay, 1967). Local, layer-parallel extension occurs in the
570 outer arc of the fold hinge in the region above the neutral surface (Fig. 20f). This stress counteracts the
571 regional stress and can produce extensional fractures or shear fractures (normal faults) both of which
572 strike parallel to the fold hinge. It is therefore possible to generate the stress regime (i.e., Fig. 20b) as a
573 local stress regime in the outer arc of a fold during the folding occurring in response to the two regional
574 stress fields (Fig. 20c & d). Below the neutral surface a local layer-parallel compression develops which
575 complements the regional stress field (Fig. 20f). This stress field could produce extensional fractures

576 parallel to the bedding or shear fractures with the orientation of thrusts (the fractures of Sets 4 and 5,
577 Fig. 20g).

578 Given the reinterpretation by the present authors that the Teton Anticlines are thrust-related
579 anticlines, then the fracture sets one would expect to encounter on these anticlines would be those
580 shown in Fig. 20d (Set 4, also Set 5, Fig. 20g) and above the neutral surface in the hinge region of the
581 anticline, those shown in Set 3 (Fig. 20b). Compression below the neutral surface in the anticline hinge
582 could generate thrusts or a disjunctive, axial planar cleavage depending on the differential stress and
583 the rock properties. In addition, because of the periclinal geometry of the anticlines there would be a
584 hinge-parallel stretching generated above the neutral surface which could generate extensional
585 fractures normal to the hinge, i.e. a set of cross axial fractures. However, the conjugate fracture set 1,
586 which require the vertical stress to be σ_2 , (Fig 20c) is not predicted by fold-related stresses for the Teton
587 anticline, where the vertical stress is σ_3 . In the authors' interpretation, two of the transverse fracture
588 sets are pre-folding. These fractures are favorably oriented for reactivation as wrench faults during later
589 fold tightening, which resulted in the development of sub-horizontal lineations on the fracture surfaces
590 which may explain the earlier interpretation of these features as a conjugate set of shear fractures.

591 Our observations indicate that the fracture development around the Teton and Little Teton
592 anticlines can be explained more accurately by a multi-stage model of fracture and fold development
593 that includes a pre-folding fracturing stage, the development and amplification of a complex forced-fold
594 pair, and late stage reactivation of some extensional fracture sets as faults, once fold amplification and
595 linkage has occurred. Thus, we consider that the fracture sets around the TA are not the result of four
596 unique stress states, each characterized by a differential stress capable of generating shear fractures
597 (Stearns, 1968) but the sequential result of multiple stages of deformation in the region since the late
598 Jurassic. This style of interpretation of fracture networks, that is, in stages including deformation prior
599 to the development of large-scale structures, is also invoked in a number of other studies, including, but
600 not limited to Bellahsen et al. (2006) and Mynatt et al. (2009).

601

602 **8. Conclusions**

603 This study has considered the brittle structures developed around the Teton and Little Teton
604 anticlines in the light of a revised understanding of the geometry and development of the anticlines
605 which are now known to be thrust related folds rather than the classical buckle folds assumed by earlier

606 workers. The model proposed for the fracture development around the Teton anticline invokes four
607 stages of structural development in this region. The first stage consists of fractures developing under a
608 regional far-field stress regime related to early Sevier orogenic deformation, before the Teton and Little
609 Teton anticlines begin to develop. The second and third stages consist of early-stage fold amplification
610 and linkage, with the development of fracture sets related to a more local stress field, which evolves as
611 the folds continue to amplify and propagate. The fourth and final stage includes continued shortening
612 across TA by the development of pronounced asymmetry and the development of accommodation
613 structures such as the wrench faults (reactivated extensional fractures) found in the south of the study
614 area where the anticline has experienced maximum amplification.

615 This reinterpretation of the classic model of fracture development linked to the growth of a
616 buckle fold has indicated that it is unlikely that all four sets of fractures proposed by Stearns will develop
617 during the evolution of an anticline. Since many fracture interpretation, modelling or prediction studies
618 still use the original model, our work suggests that it is time for a paradigm shift in the way that the
619 hydrocarbon industry approaches fracture prediction. Our results indicate that fracture networks
620 should be interpreted and characterized in light of the tectonic setting and genetic or geologic history of
621 the system as a whole, rather than solely by geometric relationship. Further implications of this result
622 are that fracture modelling by stochastic methods that do not take into account multiphase
623 deformation, potential reactivation of fractures in changing stress fields, and the potential for regional
624 deformation caused by far-field stresses may be oversimplified.

625

626 **9. Acknowledgements**

627 Support for this work came from Penn State's Appalachian Basin Black Shale Project (ABBSEG), a Janet
628 Watson Scholarship from Imperial College, London, a Geological Society of London grant for fieldwork
629 and an AAPG Susanne Takken Memorial Grant. We thank Rick Allmendinger for the use of the Stereonet
630 software, which was used to create the pole figures. We thank Tricia Allwardt, Richard Groshong, P.J.
631 Lovely, Sando Serra and two anonymous reviewers for detailed comments on earlier versions of this
632 manuscript. T.E. would like express his profound appreciation to David Stearns as a mentor in the field
633 while they were both at Texas A & M University.

634

635

636 **10. References**

- 637 Ahmadhadi, F., Lacombe, O., and Daniel, J.-M., 2007, Early reactivation of basement faults in Central
638 Zagros (SW Iran): evidence from pre-folding fracture populations in Asmari Formation and lower
639 Tertiary paleogeography, *Thrust Belts and Foreland Basins*, Springer, p. 205-228.
- 640 Belayneh, M. & Cosgrove, J.W., 2004. Fracture-pattern variations around a major fold and their
641 implications regarding fracture prediction using limited data: an example from the Bristol
642 Channel Basin. *In* Cosgrove, J.W. & Engelder, T. (eds) *The initiation, propagation and arrest of*
643 *joints and other fractures*, Geological Society of London Special Publication 231, p. 89-102
- 644 Bellahsen, N., Fiore, P. & Pollard, D., 2006. The role of fractures in the structural interpretation of Sheep
645 Mountain Anticline, Wyoming. *Journal of Structural Geology*, 28 (5) p. 850-867
- 646 Bergbauer, S., and Pollard, D. D., 2004, A new conceptual fold-fracture model including prefolding joints,
647 based on the Emigrant Gap anticline, Wyoming: *Geological Society of America Bulletin*, v. 116,
648 no. 3-4, p. 294-307.
- 649 Bessinger, B., Cook, N. G., Myer, L., Nakagawa, S., Nihei, K., Benito, P., and Suarez-Rivera, R., 2003, The
650 role of compressive stresses in jointing on Vancouver Island, British Columbia: *Journal of*
651 *structural geology*, v. 25, no. 6, p. 983-1000.
- 652 Boerner, D. E., J. A. Craven, R. D. Kurtz, G. M. Ross, and F. W. Jones, 1998, The Great Falls Tectonic Zone:
653 suture or intracontinental shear zone?: *Canadian Journal of Earth Sciences*, v. 35, p. 175-183.
- 654 Boyer, S. E., and D. Elliott, 1982, *Thrust Systems*: AAPG bulletin, v. 66, p. 1196-1230.
- 655 Casini, G., Romaine, I., Casciello, E., Saura, E., Verges, J., Fernandez, N. & Hung, D.W., in press. Fracture
656 characterization in sigmoidal folds: insights from the Siah Kuh anticline, Zagros, Iran. *AAPG*
657 *Bulletin*, DOI: 10.1306/0503171615817076
- 658 Cooper, M. 1992. The analysis of fracture systems in subsurface thrust structures from the Foothills of the
659 Canadian Rockies. *Thrust Tectonics* McClay, K.R. (ed), 391-405.
- 660 Cooper, S.P., Goodwin, L.C. & Lorenz, J.C., 2006. Fracture and fault patterns associated with basement-
661 cored anticlines: The example of Teapot Dome, Wyoming. *AAPG Bulletin*, 90 (12) p. 1903-1920.
- 662 Corbett, K., Friedman, M., and Spang, J., 1987, Fracture development and mechanical stratigraphy of
663 Austin Chalk, Texas: *AAPG Bulletin*, v. 71, no. 1, p. 17-28.

664 Cosgrove, J.W. and Ameen, M.S., 1999. A comparison of the geometry, spatial organization and fracture
665 patterns associated with forced folds and buckle folds. Geological Society of London Special
666 Publication 169, p. 7-21.

667 Crider, J., 1993, Kinematic and geometric analysis of mesoscale and macroscale brittle structures:
668 evolution of the Northern Sawtooth Range, Montana: unpublished MSc thesis.

669 Crider, J., and E. Boyer, 1993, Evidence for synchronous thrusting in the northern Sawtooth Range,
670 Montana: Abstracts with Programs - Geological Society of America, v. 25, p. 25.

671 DeCelles, P. G., 2004, Late Jurassic to Eocene evolution of the Cordilleran thrust belt and foreland basin
672 system, western USA: American Journal of Science, v. 304, p. 105-168.

673 Dickinson, W. R., and G. E. Gehrels, 2003, U-Pb ages of detrital zircons from Permian and Jurassic eolian
674 sandstones of the Colorado Plateau, USA: paleogeographic implications: Sedimentary Geology, v.
675 163, p. 29-66.

676 Engelder, T., and Geiser, P., 1980, On the use of regional joint sets as trajectories of paleostress fields
677 during the development of the Appalachian Plateau, New York: Journal of Geophysical Research,
678 v. 85, no. B11, p. 6319-6341.

679 Engelder, T., Gross, M. R., and Pinkerton, P., 1997, Joint development in clastic rocks of the Elk Basin
680 anticline, Montana-Wyoming: An analysis of fracture spacing versus bed thickness in a
681 basement-involved Laramide structure, *in* Hoak, T., Klawitter, A., and Blomquist, P., eds., Rocky
682 Mountain Association of Geologists 1997 Guidebook: Denver, Colorado, p. 1-18.

683 Finn, C. A., and P. K. Sims, 2005, Signs from the Precambrian: The Geologic Framework of Rocky Mountain
684 Region derived from Aeromagnetic Data: In Karlstrom, K.E. & Keller, G.R., (eds) The Rocky
685 Mountain Region: An evolving lithosphere, v. Geophysical Monograph 154, p. 39-54

686 Fischer, M. P., and Wilkerson, M. S., 2000, Predicting the orientation of joints from fold shape: Results of
687 pseudo-three-dimensional modeling and curvature analysis: Geology, v. 28, no. 1, p. 15-18.

688 Friedman, M. & Stearns, D. W. 1971. Relations between Stresses Inferred from Calcite Twin Lamellae and
689 Macrofractures, Teton Anticline, Montana. *Geological Society of America Bulletin* **82**(11), 3151-&.

690 Ghosh, K. & Mitra, S., 2009. Structural controls of fracture orientations, intensity and connectivity,
691 Teton anticline, Sawtooth Range, Montana, AAPG Bulletin, v93 (8) p995-1014.

692 Hennings, P. H., Olson, J. E., and Thompson, L. B., 2000, Combining outcrop data and three-dimensional
693 structural models to characterize fractured reservoirs: An example from Wyoming: AAPG
694 bulletin, v. 84, no. 6, p. 830-849.

695 Holl, J. E., and D. J. Anastasio, 1992, Deformation of a Foreland Carbonate Thrust System, Sawtooth
696 Range, Montana: Geological Society of America Bulletin, v. 104, p. 944-953.

697 Jamison, W.R., 2016. Fracture system evolution within the Cardium Sandstone, central Alberta Foothills
698 folds. AAPG Bulletin, v. 100, p. 1099-1134

699 Lacombe, O., Bellahsen, N. and Mouthereau, F., 2011. Fracture patterns in the Zagros Simply Folded Belt
700 (Fars, Iran): constraints on early collisional tectonic history and role of basement faults. Geological
701 Magazine, v. 148, p. 940-963

702 Laubach, S. E., 1992, Fracture networks in selected Cretaceous sandstones of the Green River and San
703 Juan basins, Wyoming, New Mexico, and Colorado: Rocky Mountain Association of Geologists, p.
704 61-74 .

705 Lisle, R. J. 1992. Constant bed-length folding: three-dimensional geometrical implications. Journal of
706 Structural Geology, 14, No. 2, 245-52.

707 Lisle, R. J. 1994. Detection of Zones of Abnormal Strains in Structures Using Gaussian Curvature

708 Lorenz, J. C. 1982. Lithospheric flexure and the history of the Sweetgrass Arch, NW Montana. *Rocky*
709 *Mountain of Geologists Symposium*, 77-89.

710 Lorenz, J. C., Sterling, J. L., Schechter, D. S., Whigham, C. L., and Jensen, J. L., 2002, Natural fractures in the
711 Spraberry Formation, Midland basin, Texas: The effects of mechanical stratigraphy on fracture
712 variability and reservoir behavior: AAPG bulletin, v. 86, no. 3, p. 505-524.

713 Lorenz, J. C., Teufel, L.W. & Warpinski, N.R., 1991. Regional Fractures I: A mechanism for the Formation
714 of Regional Fractures at Depth in Flat Lying Reservoirs. AAPG Bulletin, v. 75, p. 1714-1737

715 Marshak, S., Wilkerson, M., and Hsui, A., 1992, Generation of curved fold-thrust belts: Insight from simple
716 physical and analytical models, Thrust tectonics, Springer, p. 83-92.

717 McConaughy, D. T., and Engelder, T., 1999, Joint interaction with embedded concretions: joint loading
718 configurations inferred from propagation paths: Journal of Structural Geology, v. 21, no. 11, p.
719 1637-1652.

720 McQuillan, H., 1973, Small-scale fracture density in Asmari Formation of southwest Iran and its relation
721 to bed thickness and structural setting: AAPG Bulletin, v. 57, no. 12, p. 2367-2385.

722 Mudge, M. R., 1970, Origin of Disturbed Belt in Northwestern Montana: Geological Society of America
723 Bulletin, v. 81, p. 377-392.

724 Mudge, M. R., 1982a, A resume of the structural geology of the northern disturbed belt, NW Montana:
725 Geologic Studies of the Cordilleran Thrust belt v. Powers, R.B. (ed), p. 91-122.

726 Mudge, M. R., 1982b, Geologic and structure map of the Choteau 1 x 2 degree quadrangle, Western
727 Montana: USGS Miscellaneous Investigations Series, v. I-1300.

728 Mudge, M. R., and R. L. Earhart, 1983, Bedrock geologic map of part of the northern disturbed belt, Lewis
729 and Clark, Teton, Pondera, Glacier, Flathead, Cascade, and Powell Counties, Montana: U.S.
730 Geological Survey Miscellaneous Investigations I-1375.

731 Muecke, G.K. & Charlesworth, H.A.K., 1966. Jointing in folded Cardium Sandstones along the Bow River,
732 Alberta. Canadian Journal of Earth Sciences, v. 3, p. 579-596

733 Mynatt, I., Seyum, S. & Pollard, D. 2009. Fracture initiation, development, and reactivation in folded
734 sedimentary rocks at Raplee Ridge, UT. Journal of Structural Geology, 31 (10) p1100-1113.

735 O'Neill, J. M., and D. A. Lopez, 1985, Character and Regional Significance of Great Falls Tectonic Zone, East
736 Central Idaho and West-Central Montana: Aapg Bulletin-American Association of Petroleum
737 Geologists, v. 69, p. 437-447.

738 Pollard, D. D., and Aydin, A., 1988, Progress in understanding jointing over the past century: Geological
739 Society of America Bulletin, v. 100, no. 8, p. 1181-1204.

740 Ramsay, J.G., 1967. Folding and Fracturing of Rocks. McGraw-Hill, New York. 568pp

741 Reinecke, K. M. 1989. Effect of Scapegoat-Bannatyne trend on the structural development of the
742 Montana Disturbed Belt. Montana Geological Society field conference, 249-260.

743 Sando, W. J. 1976. Mississippian History of Northern Rocky Mountains Region. *Journal of Research of the*
744 *Us Geological Survey* 4(3), 317-338.

745 Sanz, P. F., Pollard, D. D., Allwardt, P. F., and Borja, R. I., 2008, Mechanical models of fracture reactivation
746 and slip on bedding surfaces during folding of the asymmetric anticline at Sheep Mountain,
747 Wyoming: *Journal of Structural Geology*, v. 30, p. 1177-1191.

748 Silliphant, L. J., Engelder, T., and Gross, M. R., 2002, The state of stress in the limb of the Split Mountain
749 Anticline, Utah; constraints placed by transected joints: *Journal of Structural Geology*, v. 24, no.
750 1, p. 155-172.

751 Singdahlsen, D. S. 1984. Structural Geology of Swift Reservoir Culmination, Sawtooth Range, Montana.
752 AAPG Bulletin-American Association of Petroleum Geologists 68(7), 949-949.

753 Smart, K.J., Ferrill, D.A. & Morris, A.P., 2009. Impact of interlayer slip on fracture prediction from
754 geomechanical models of fault-related folds. AAPG Bulletin v. 93, p. 1447-1458

755 Spang, J.H., 1972, Numerical method for dynamic analysis of calcite twin lamellae: *Geological Society of*
756 *America*, v. 83, p. 467-472.

757 Srivastava, D. C., and Engelder, T., 1990, Crack-propagation sequence and pore-fluid conditions during
758 fault-bend folding in the Appalachian Valley and Ridge, central Pennsylvania: *Geological Society*
759 *of America Bulletin*, v. 102, no. 1, p. 116-128.

760 Stearns, D.W. 1964. Macrofracture patterns on Teton Anticline, northwest Montana. *Transactions of*
761 *the American Geophysical Union*, 45, 107-108

762 Stearns, D. W. 1968. Certain aspects of fracture in naturally deformed rocks. In Reicker, R.E. (ed)
763 *Advanced Science Seminar in Rock Mechanics*, Air Force Cambridge Research Laboratory.

764 Suppe, J., 1983, Geometry and kinematics of fault-bend folding: *American Journal of Science*, v. 283, no.
765 7, p. 684-721.

766 Suppe, J. 1985. *Principles of Structural Geology*. Prentice-Hall, Englewood Cliffs, NJ.

767 Tamara, J., Mora, A., Robles, W., Kammer, A., Ortiz, A., Sanchez-Villar, N., Piraquive, A., Rueda, L. H.,
768 Casallas, W., and Castellanos, J., 2015, Fractured reservoirs in the Eastern Foothills, Colombia,
769 and their relationship with fold kinematics: AAPG Bulletin, v. 99, no. 8, p. 1599-1633.

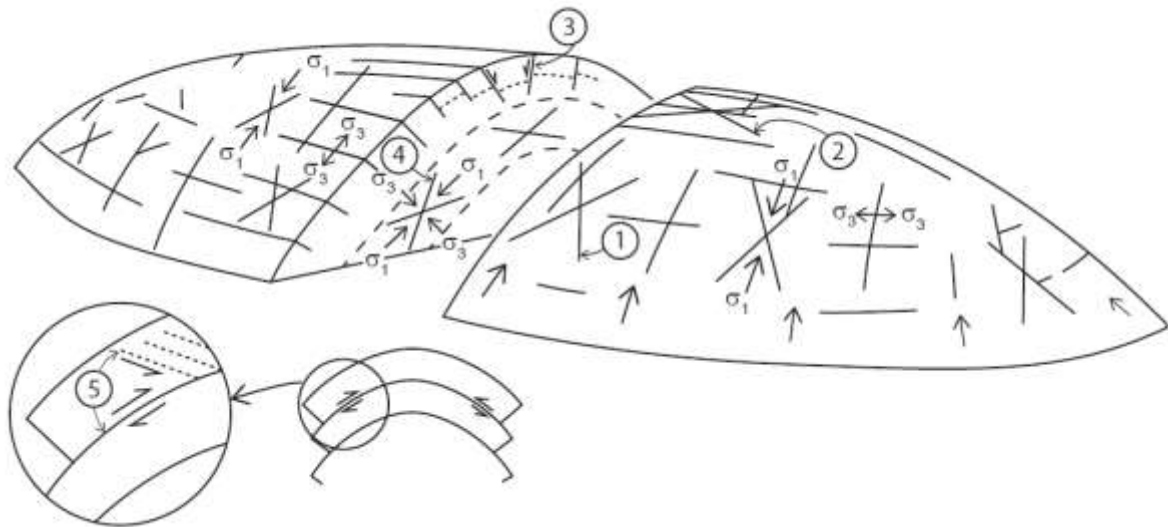
770 Watkins, H., Healy, D., Bond, C.E. & Butler, R.W.H., in press. Implications of heterogeneous fracture
771 distribution on reservoir quality: an analogue from the Torridon Group sandstone, Moine Thrust
772 Belt, NW Scotland. *Journal of Structural Geology*, doi: 10.1016/j.jsg.2017.06.002

773 Watkins, H., Butler, R.W.H., Bond, C.E. & Healy, D., 2015. Influence of structural position on fracture
774 networks in the Torridon Group, Achnashellach fold and thrust belt, NW Scotland. Journal of
775 Structural Geology, v.74, p. 64-80.

776 Younes, A. I., and Engelder, T., 1999, Fringe cracks; key structures for the interpretation of the
777 progressive Alleghanian deformation of the Appalachian Plateau: Geological Society of America
778 Bulletin, v. 111, no. 2, p. 219-239.

779

780 **Teton Figures and Captions**

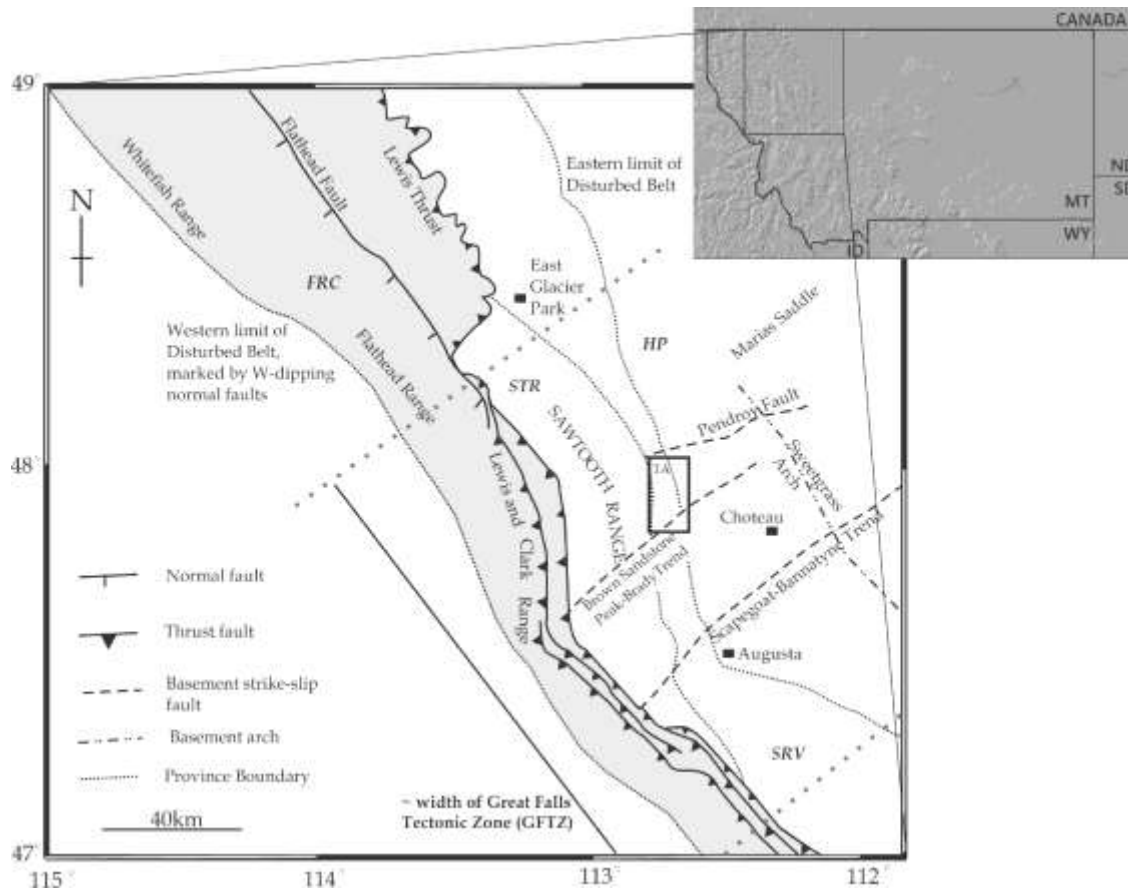


781

782

783 Figure 1: Diagram of a pericline showing the 5 sets of conjugate shear fractures and their associated
784 extensional fractures, identified by Stearns 1968 and subsequent authors based on their study of the Teton
785 anticline.

786



787

788 Figure 2: Location map, showing the Sawtooth Range at the leading edge of the Sevier Orogen, with an inset

789 showing the location of the Sawtooth Range in Montana. The inset basemap is from GeoMapApp.

790 The boxed area shows the location of the study area and extent of the map in Figure 3. Modified after

791 Mudge, 1982b. TA – Teton anticlines, gray area – Proterozoic rocks of the Lewis thrust sheets. The

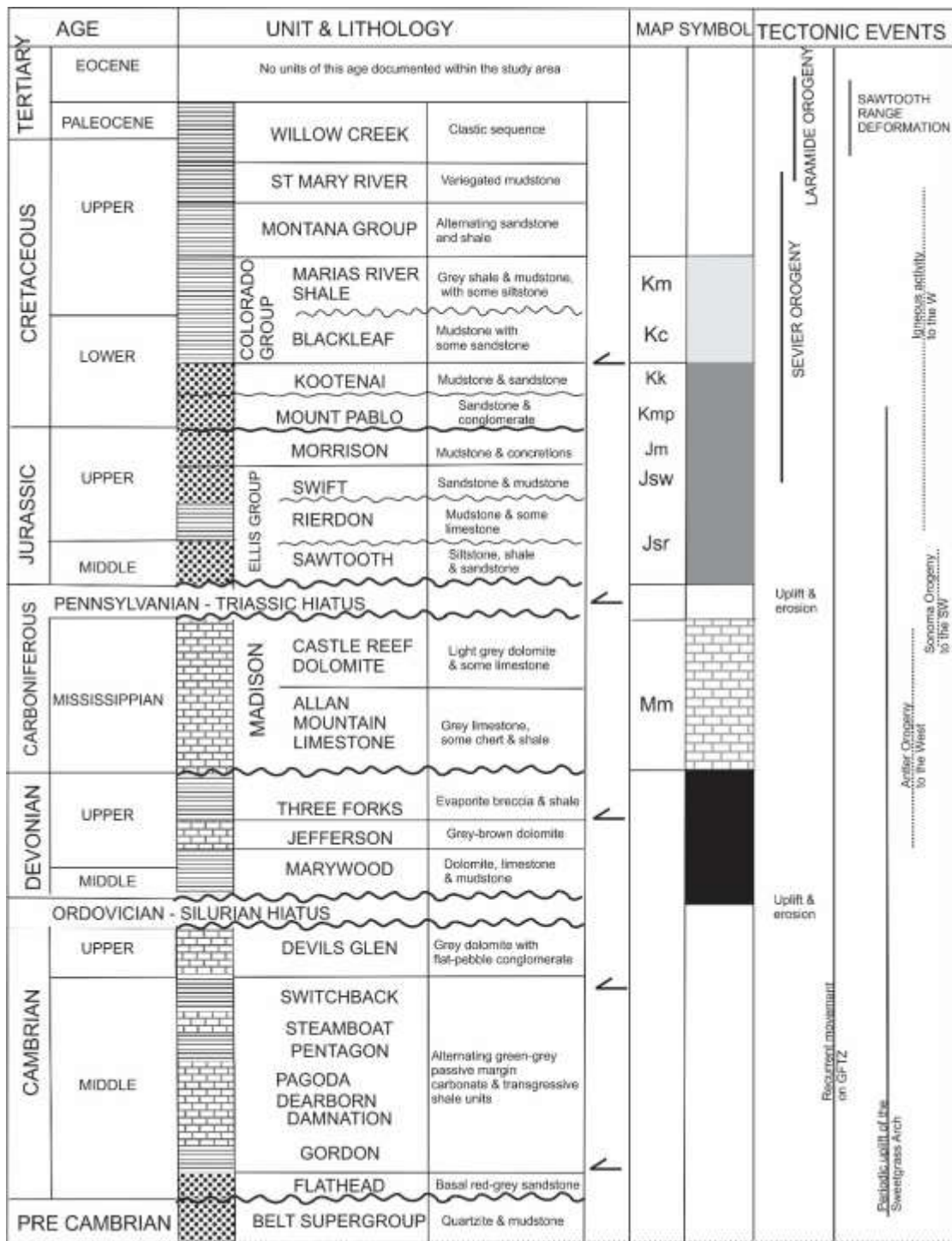
792 locations of key basement lineaments which trend approximately NE-SW are shown as dashed lines.

793 The area is divided into four provinces which are parallel to the deformation belt. HP – High Plains

794 province, SRV – Sun River Valley Province, STR – Sawtooth Range Province, FRC – Flathead Range

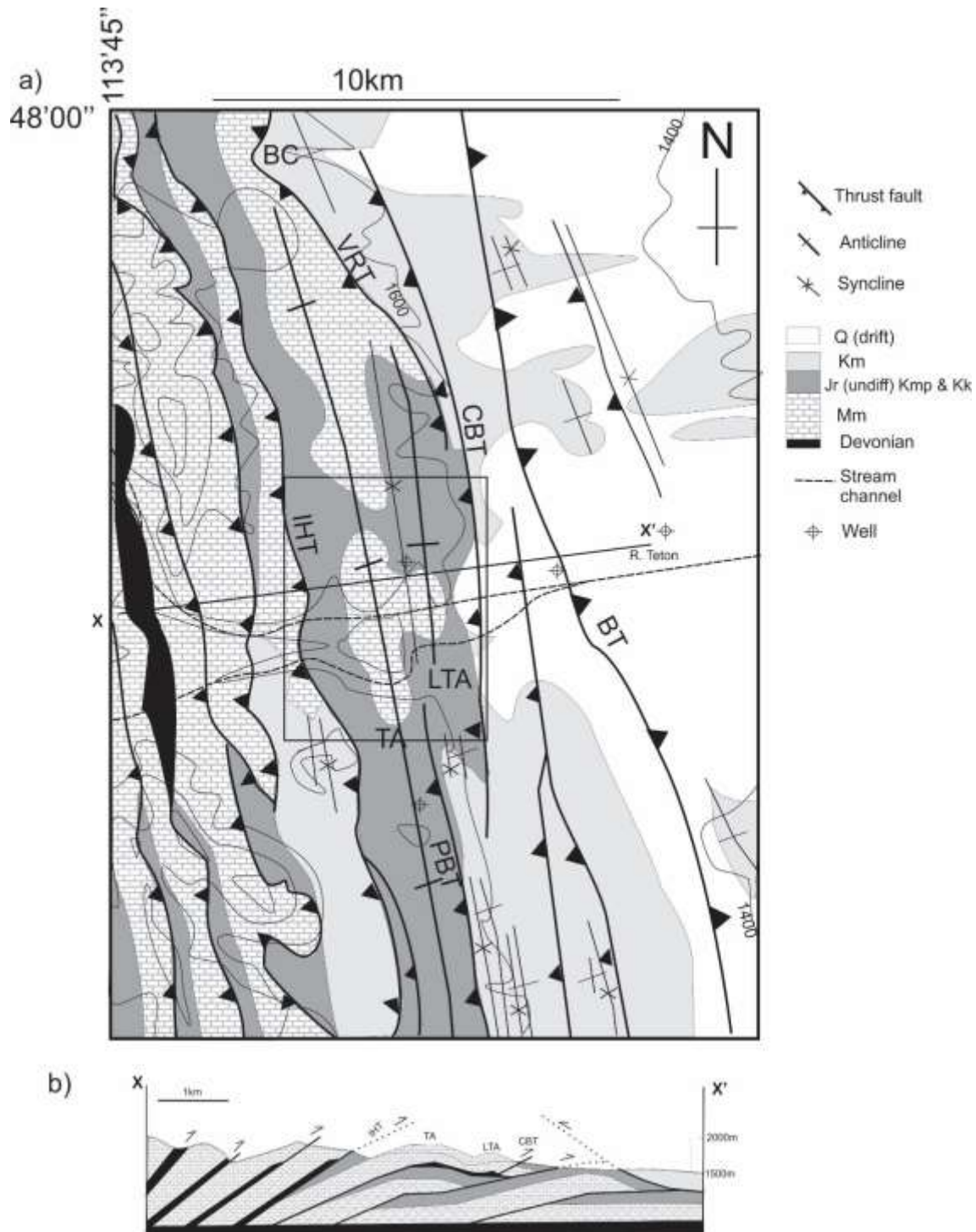
795 Province

796



797

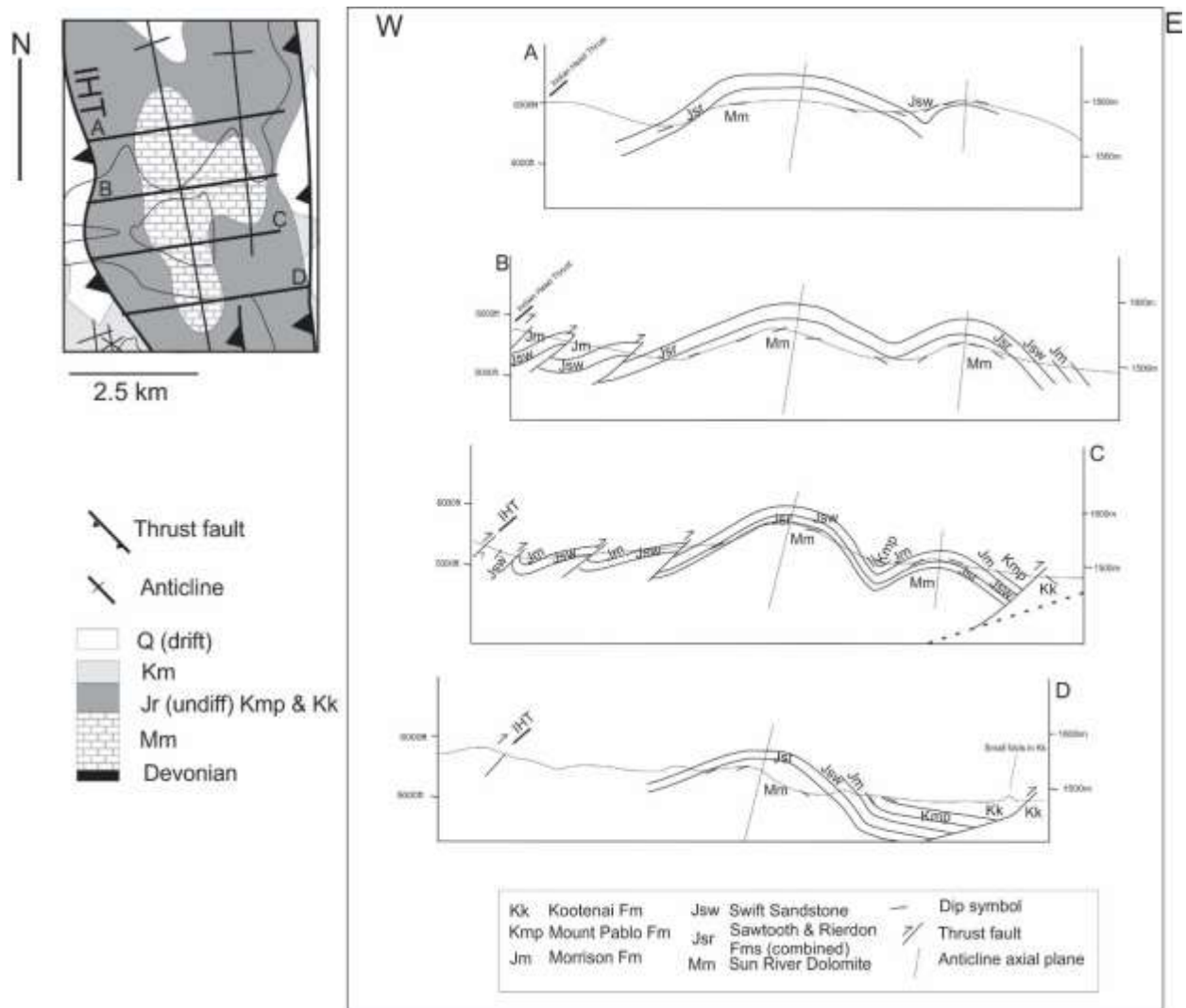
798 Figure 3: Tectonostratigraphic column illustrating the evolution of the Sawtooth Range and the associated
 799 sedimentary units from the Precambrian to the Eocene. The map symbols are those used in Figure 3.
 800 This is a summary figure based upon references cited within the text. The half arrows indicate the
 801 horizons within the column where major detachments formed.



802

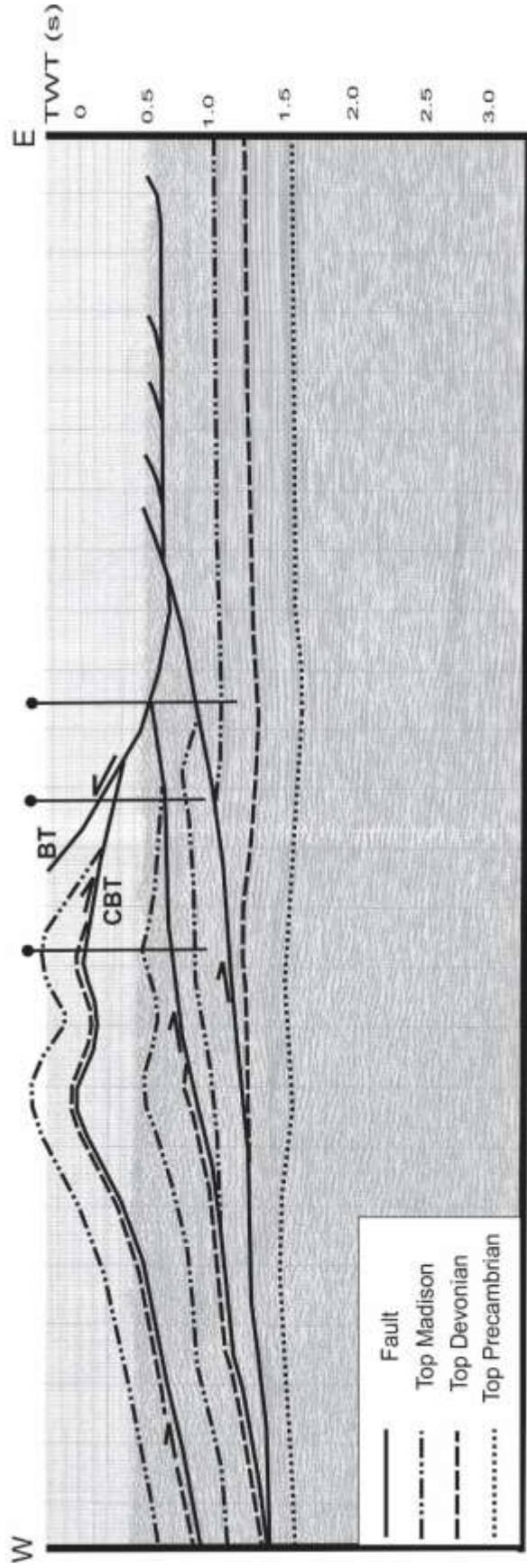
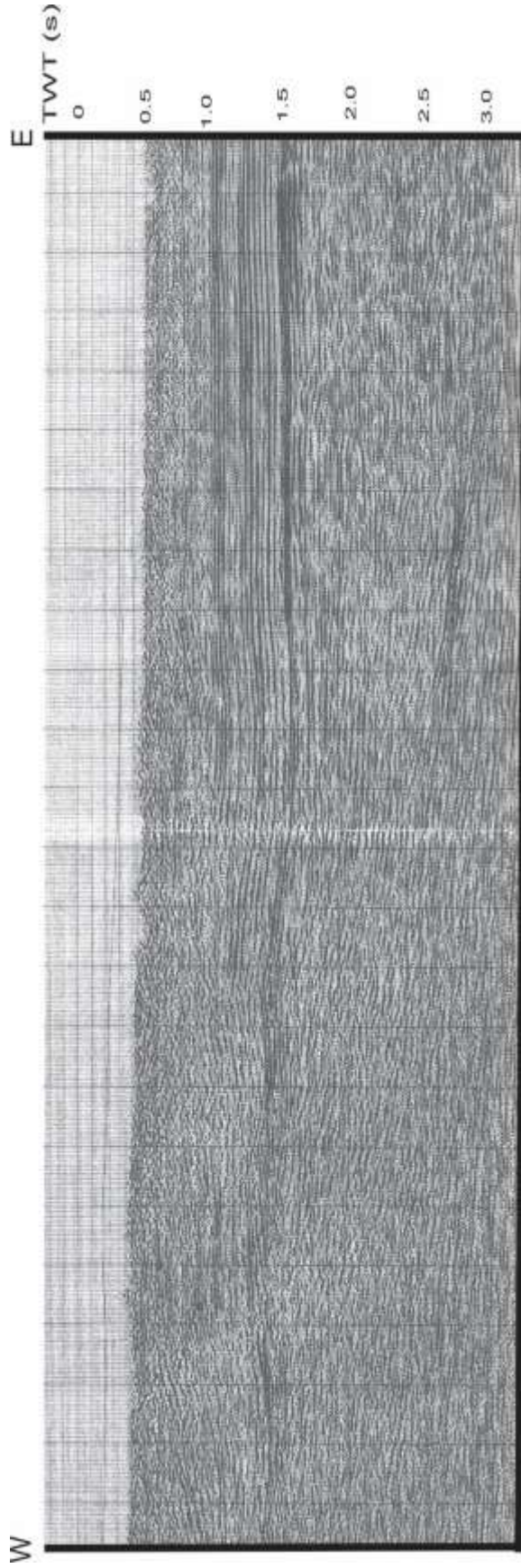
803 Figure 4: a) Geologic map of the Teton Canyon area, showing two fold structures close to the deformation
 804 front. BC – Blackleaf Canyon, IHT - Indian Head Thrust, PBT – Pine Butte Thrust, VRT – Volcano
 805 Reef Thrust,– CBT – Crab Butte Thrust, BT – Blixrud backthrust, TA - Teton anticline, LTA – Little
 806 Teton anticline. . Contours are in m above sea level and spacing is 200m. The location of the cross-

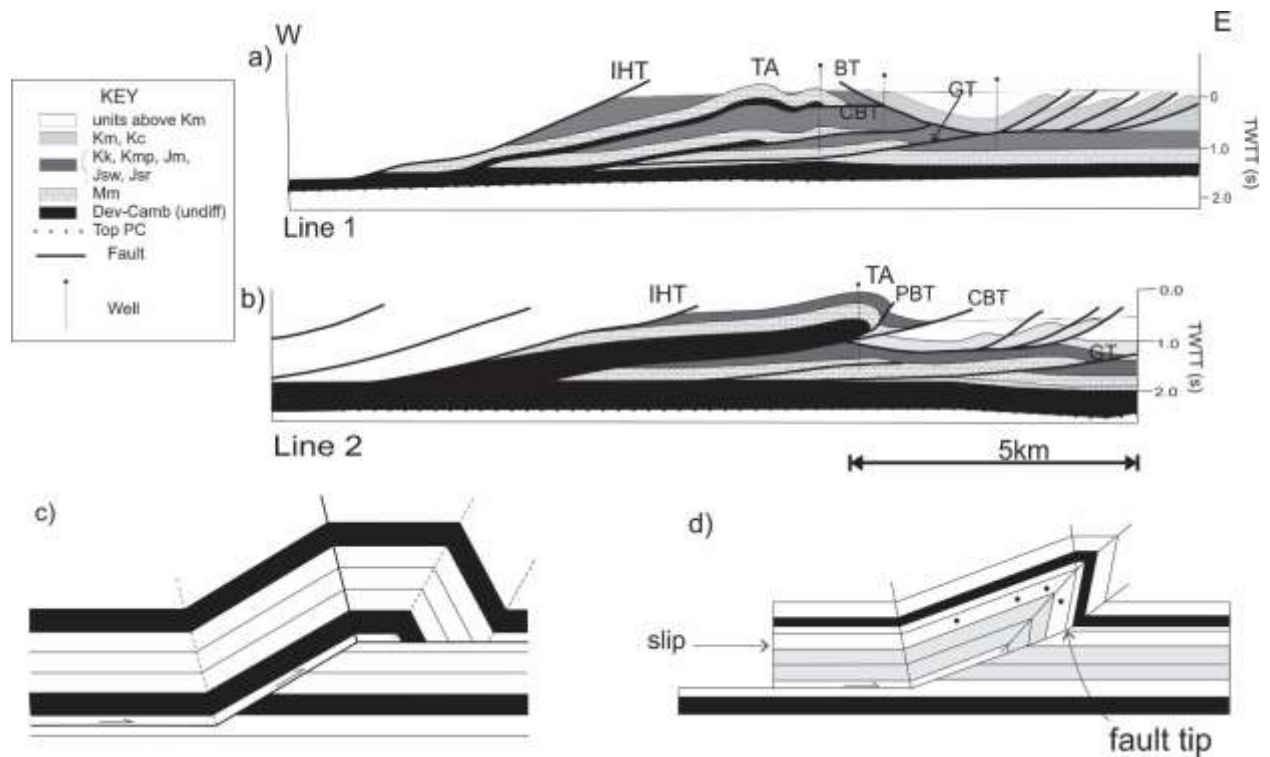
807 section (part b) is marked as X-X' and the boxed area shows the area considered in this study. This is
 808 also the location of the simplified map in Figure 5. Modified after Mudge 1982a.



809
 810 Figure 5: Cross sections based on structural data collected from across the mapped region of the Teton
 811 anticlines, showing the change in dip of the fold limbs as the fold is traced southwards. The location
 812 of each cross-section is shown on the simplified map, reproduced from the central portion of Figure
 813 3. The marker layer used and marked in these sections is the “Jsr” unit, see Fig. 2.

814
 815
 816 Figure 6 (next page) : Interpreted seismic line from the Teton Canyon region, crossing the northern section of
 817 the fold (close to Line X-X' in Figure 3 and Line B in Figure 4) and showing the three major thrust
 818 sheets beneath the fold structures. A backthrust can be interpreted from well data constraints.



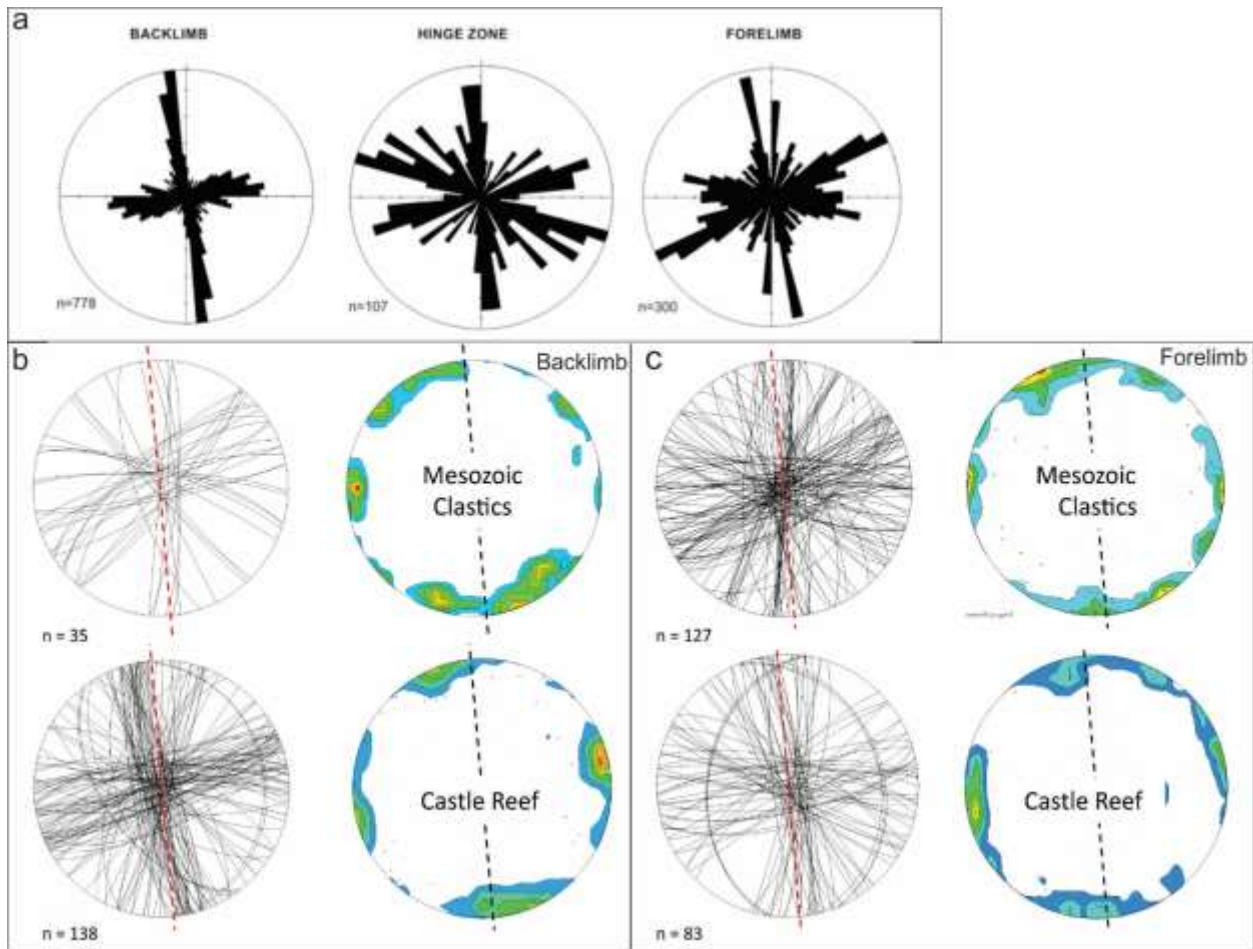


820

821

822 Figure 7: a) and b) Two interpreted seismic lines (data courtesy of SEI) across the Teton anticline. Line 1 is
 823 located close to line X-X' in Fig. 4 and Line B in Fig. 5, and is the line shown in Fig. 6. Line 2 is located
 824 south of the study area (see Fig. 4) i.e. south of the section shown in Fig. 5d. CBT – Crab Butte Thrust,
 825 PBT – Pine Butte Thrust, IHT – Indian Head Thrust, TA – Crest of Teton anticline, BT – Blixrud
 826 Thrust, GT – Gleason Thrust. c) shows the geometry of an idealized fault-bend fold, (after Suppe
 827 1985). d) shows the geometry of an idealized fault propagation fold (after Medwedeff 1990).

828



829

830 Figure 8: Fracture orientation data from the northern traverse of Teton anticline. Presentations include lower
 831 hemisphere projections of fractures fracture planes, contoured projections of poles to fractures, and
 832 rose diagrams. The data are sorted by structural position on the fold and include the backlimb, hinge
 833 zone, nose, and forelimb and rotated to horizontal. Contours to poles is in %/1% area with the
 834 contour interval at 2%. The number to the bottom left of each diagram denotes the number of data
 835 points in the stereonet or rose diagram. The dashed lines represent the trend of the fold axes.

836

837

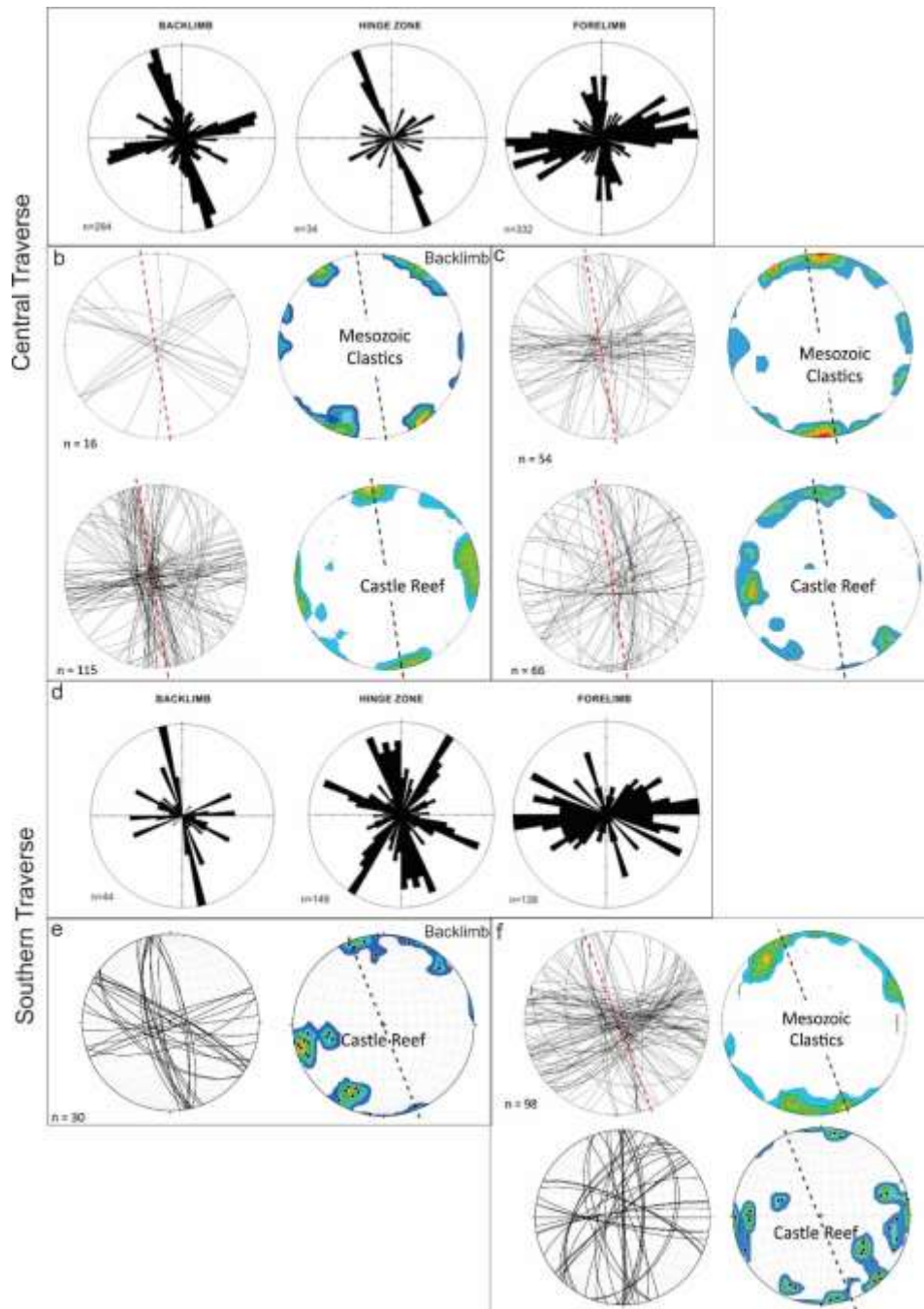


838

839 Figure 9: Abutting relationship between the joint sets on the crest of the Teton Anticline. a). joint sets ~110
 840 and ~170 abut the 085 set. b). joint sets ~110 and ~170 also abut the ~065 set. The relationship
 841 between the ~065 and ~085 sets is unclear on the end of the northern traverse (fig 5A).

842

843



844

845 Figure 10: Fracture orientation data from two additional traverses of Teton anticline (a-c, Central; d-f,
 846 Southern). Presentations include lower hemisphere projections of fracture planes, contoured
 847 projections of poles to fractures, and rose diagrams. The data are sorted by structural position on the
 848 fold and include the backlimb, hinge zone, nose, and forelimb and rotated to horizontal. Contours to
 849 poles is in %/1% area with the contour interval at 2%. The number to the bottom left of each diagram
 850 denotes the number of data points in the stereonet or rose diagram. The dashed lines represent the
 851 trend of the fold axes.



852

853

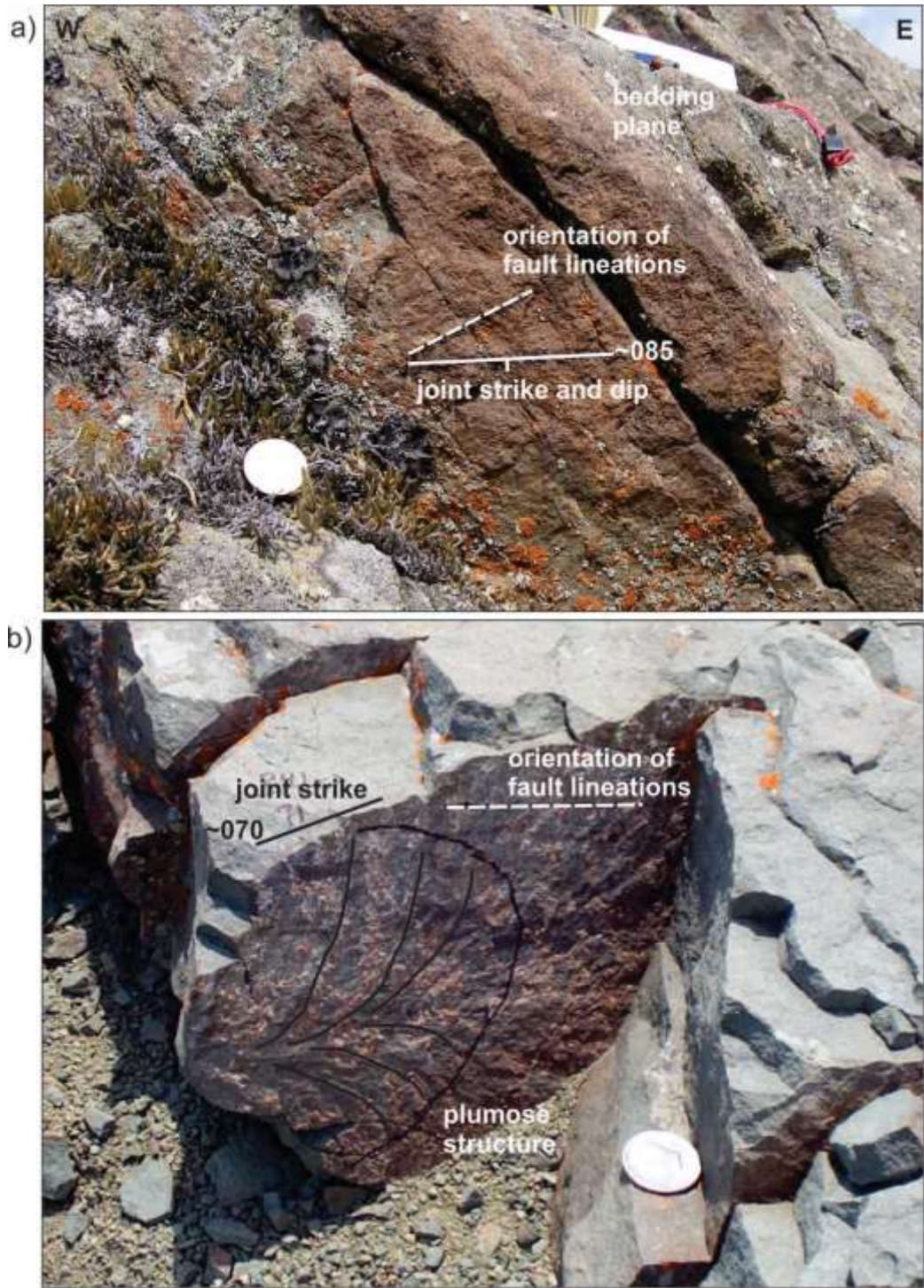
854

Figure 11: a) An aerial photograph showing the North Fork and South Fork tributaries of the Teton River.

The Little Teton anticline dies out between the two forks. Major fractures are picked out on the

855
856

Teton anticline by lines of trees b) view looking W towards the forelimb of the Teton anticline in its central section. Note the lines of trees picking out the major fractures.

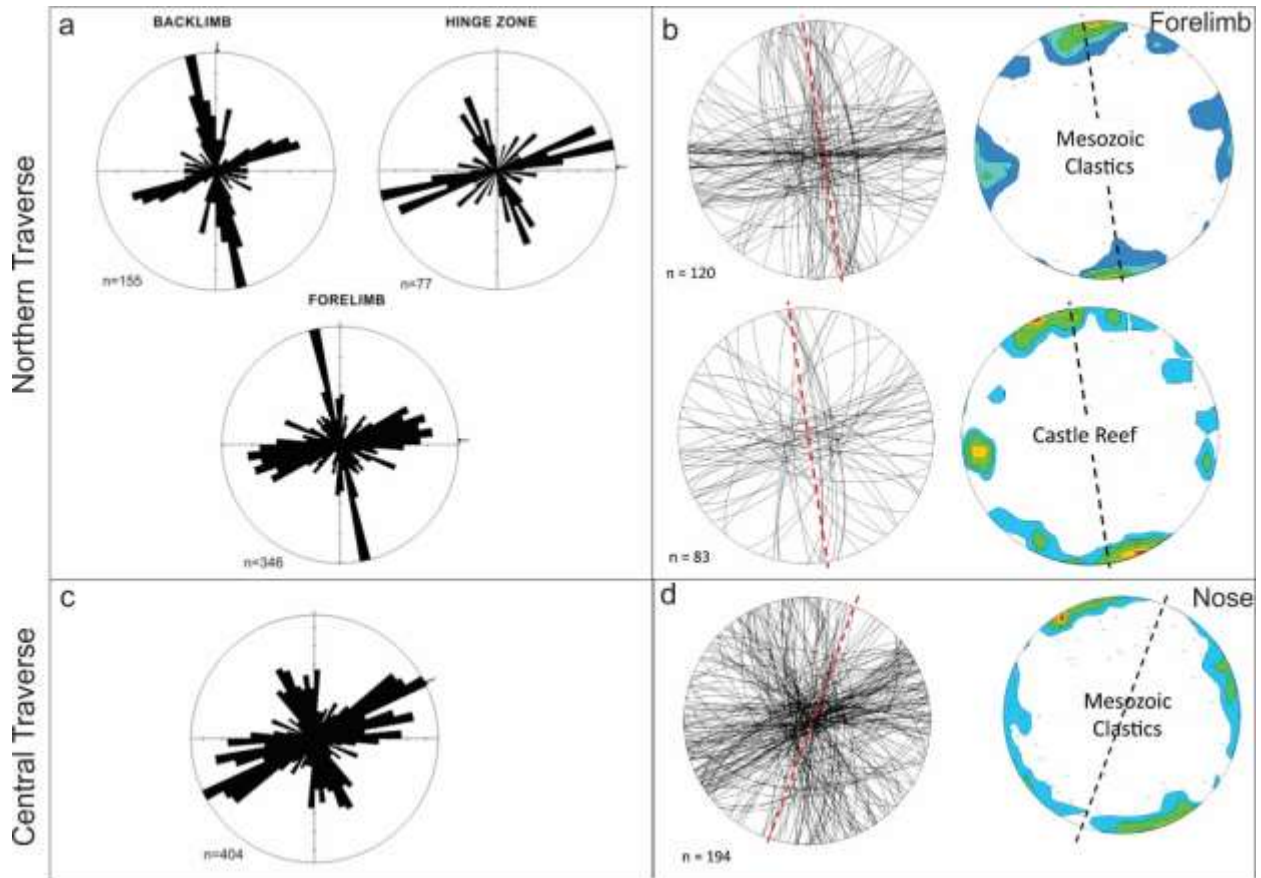


857

858 Figure 12: a) mineral lineations developed on a vertical fracture with the same strike as the transverse joints,
859 indicating that sub-horizontal slip has occurred on this surface, b) mineral lineations overprinting a

860 plumose structure on a second transverse joint, indicating that the surface developed as an opening-
861 mode joint and was later reactivated with sub-horizontal slip.

862



863

864 Figure 13: Fracture orientation data from two traverses of Little Teton anticline. Presentations include lower
865 hemisphere projections of fracture planes, contoured projections of poles to fractures, and rose
866 diagrams. The data are sorted by structural position on the fold and include the backlimb, hinge zone,
867 nose, and forelimb and rotated to horizontal. Contours to poles is in %/1% area with the contour
868 interval at 2%. The number to the bottom left of each diagram denotes the number of data points in
869 the stereonet or rose diagram. The dashed lines represent the trend of the fold axes.

870



871

872 Figure 14: Field photographs of joints contained within concretions of the Morrison Formation. Quarter
873 dollar coin for scale. a). ~065 joint abuts a prominent ~085 joint. The ~ 065 joint is also seen to
874 continue outside the concretion whereas the ~085 joint cannot be seen in the matrix . b). An ~065
875 joint cutting both the concretion and the matrix of the Morrison Formation. In contrast the ~085
876 joints are contained within the concretion.

a



b

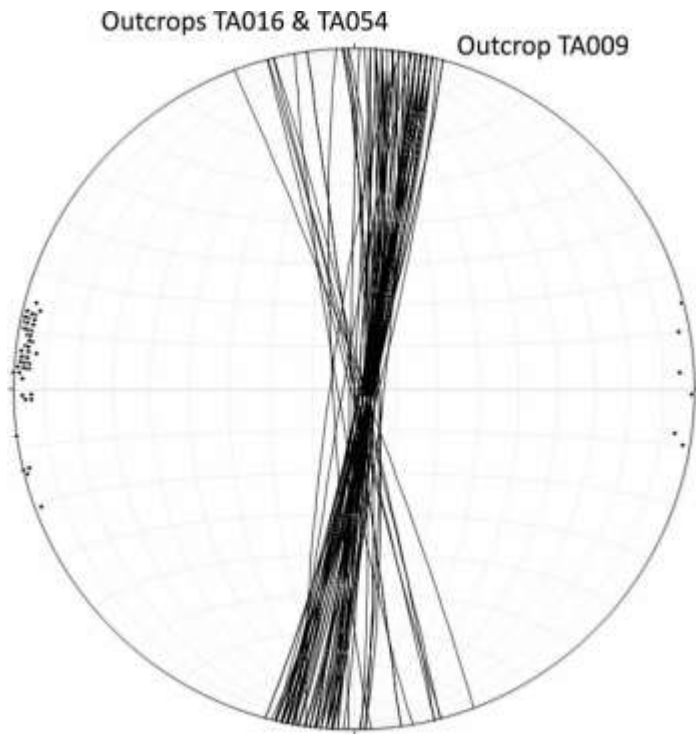


877

878 Figure 15. a) Disjunctive cleavage developed in the core of the Teton Anticline. b) Small-scale thrusts
879 developed in the core of the Teton Anticline.

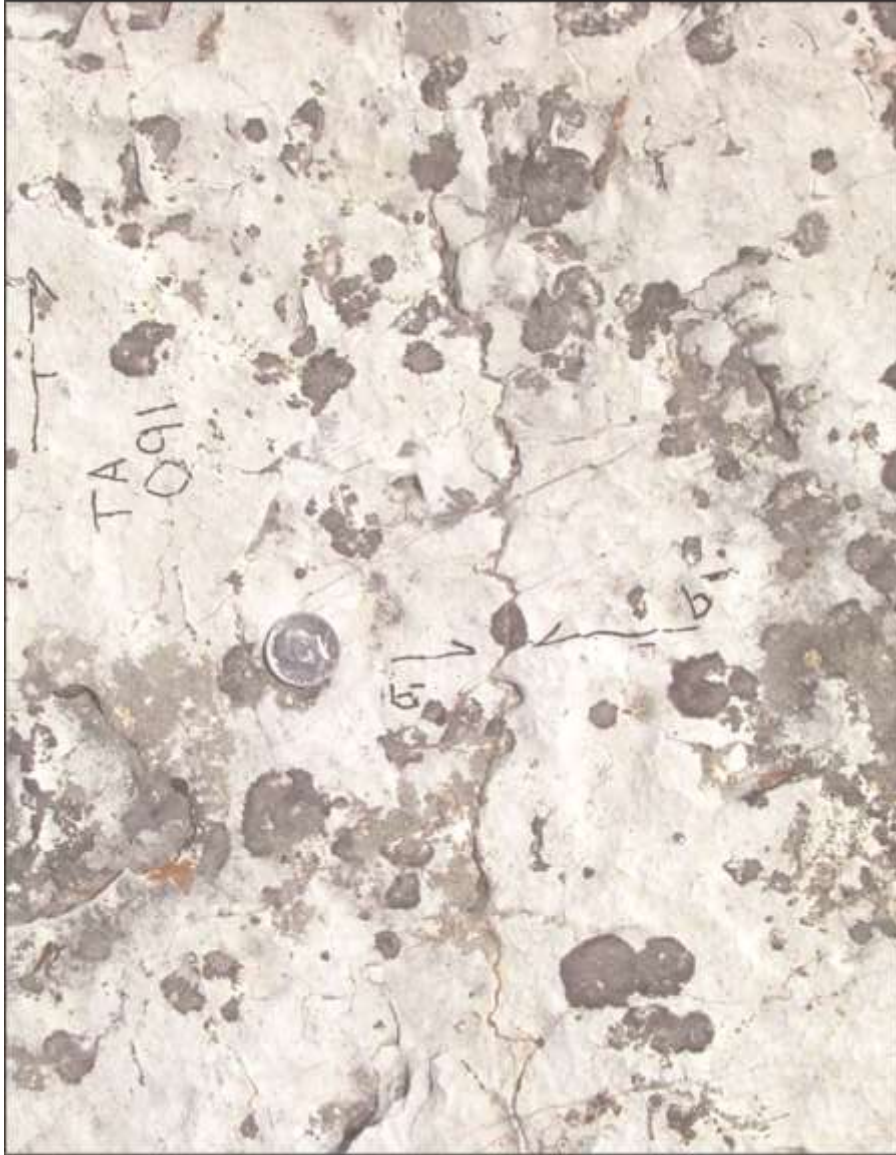
880

881



882

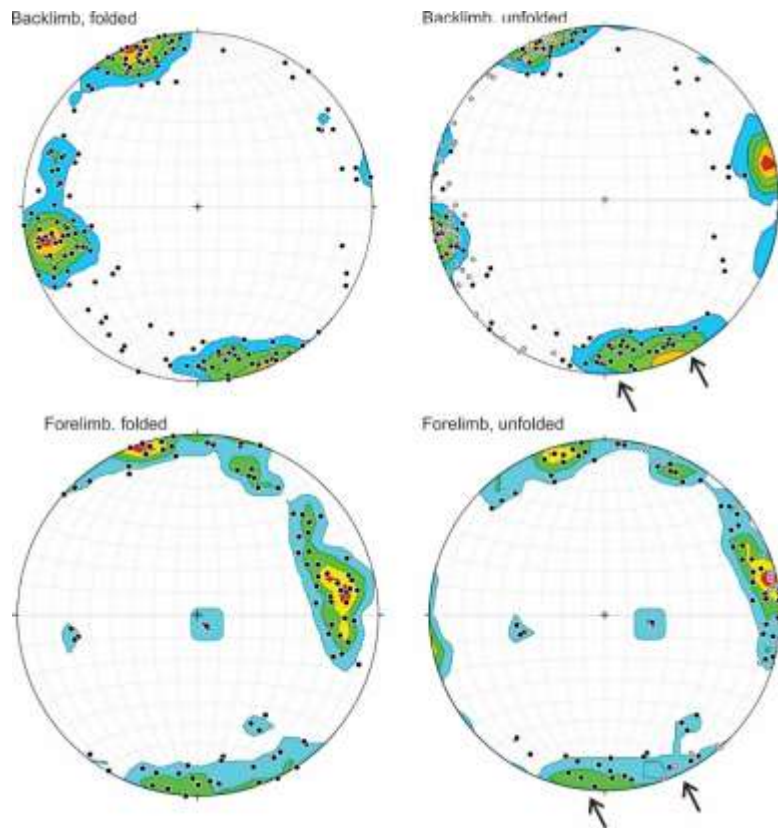
883 Figure 16: Disjunctive cleavage within the Madison Formation plotted as both poles and planes.



884

885 Figure 17. A view of a bedding plane showing mini-joints developed around a bedding-normal stylolite
886 formed parallel to the axial plane of the anticline in the Madison Formation exposed in the hinge
887 zone. Quarter dollar coin for scale. The image has been artificially lightened to enhance the visibility
888 of the small, low aperture mini-joints. North is to the top of the image.

889



890

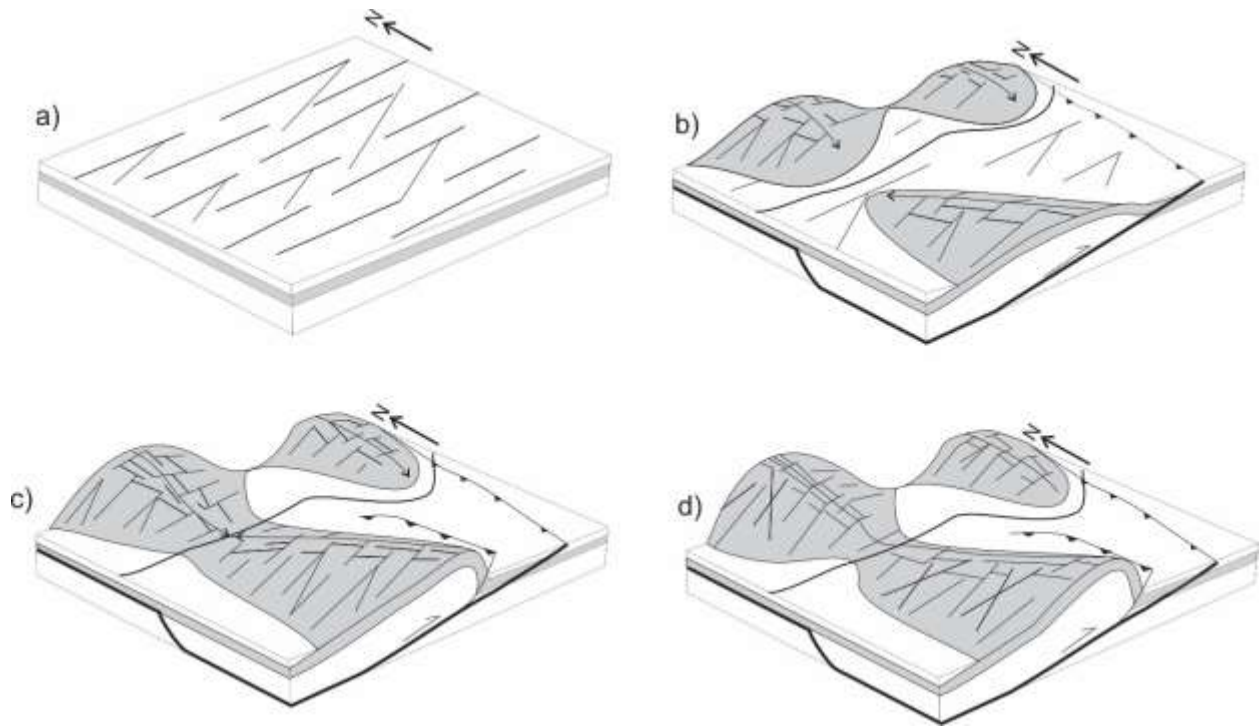
891

892 Figure 18. The “fold test” for the Northern Traverse of TA. Data from forelimb and backlimb are shown.
 893 The folded data show loose clustering for the transverse set, and a relatively clear cluster for the longitudinal
 894 set. In contrast, on unfolding, the transverse set remains loosely clustered, in one case with several sub-peaks
 895 (arrowed) and the longitudinal set becomes more dispersed. This implies that some of the transverse
 896 orientations are pre-folding.

897

898

899



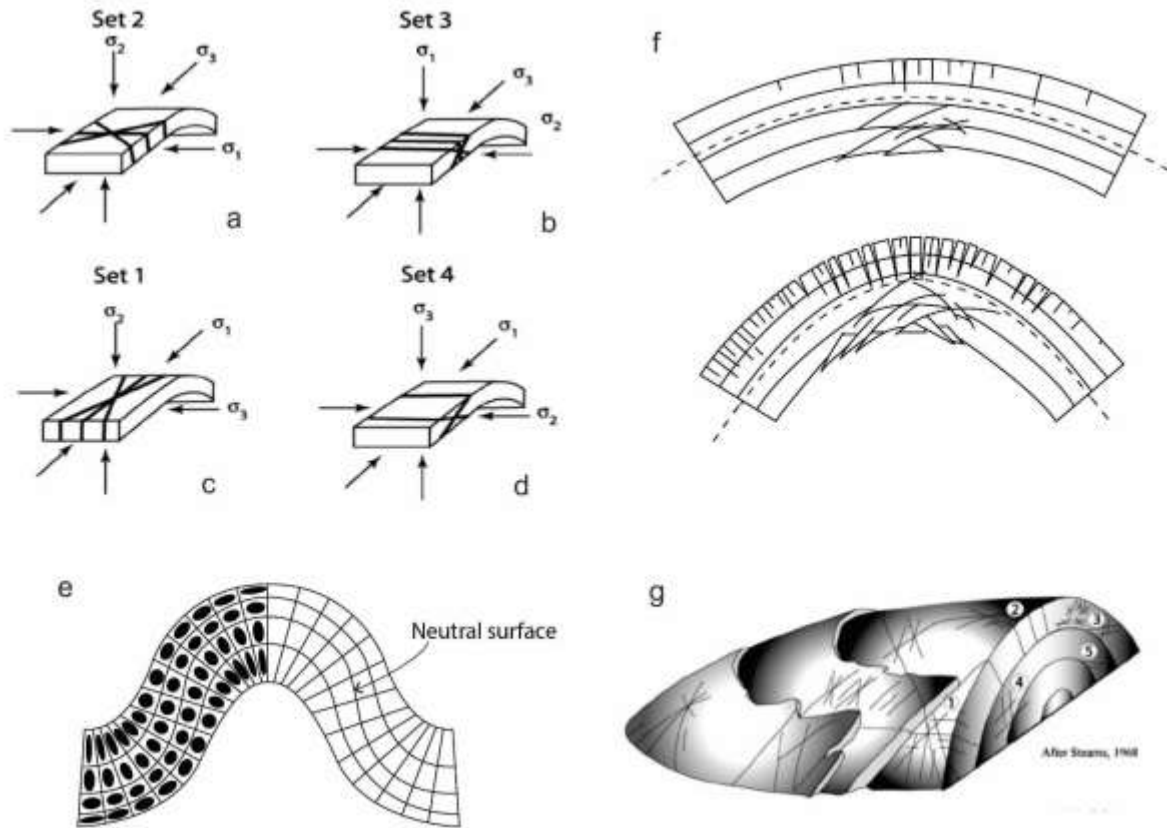
900

901 Figure 19: Block diagrams illustrating the main stages in the development of the fracture patterns and the
 902 associated Teton anticlines at the deformation front of the Sawtooth Range. A) Development of 2 pre-
 903 folding, regional fracture sets across the region B) Separate folds propagate towards each other, with
 904 the development of longitudinal joints in the hinge regions; C) folds link up and propagation ceases,
 905 longitudinal joints continue to develop; D) additional shortening is accommodated by tightening of the
 906 linked zone and the development of wrench movement on favorably oriented joints (X shape). The
 907 thrust sheet shown with a heavy line is the CBT. For clarity, the underlying thrust sheets are not
 908 shown. Fractures developing during each stage are shown with heavier lines than fractures being
 909 passively transported in the folded beds.

910

911

912



913

914 Figure 20: (a – d) Fracture sets as described by Stearns (1968) which he found associated with the Teton
 915 anticline. The diagrams show the orientation of the major fractures with respect to the fold geometry, and the
 916 orientations of the three principal stresses responsible for the fractures. e: The strain distribution likely to
 917 develop in an isotropic homogeneous bed during folding. The model is termed a Tangential Longitudinal
 918 Strain fold (TLS). f) Some possible fractures formed in the hinge region of open and more closed TLS folds
 919 (e & f after Ramsay 1967) g) An idealized pericline on which has been superimposed the fracture sets shown
 920 in (a – d) (modified from Stearns 1968).

921

922